2
Physical Methods for Characterizing Solids

2.1 INTRODUCTION

A vast array of physical methods are used to investigate the structures of solids, each technique with its own strengths and weaknesses—some techniques are able to investigate the local coordination around a particular atom or its electronic properties, whereas others are suited to elucidating the long-range order of the structure. No book could do justice to all the techniques on offer, so here we describe just some of the more commonly available techniques, and try to show what information can be gleaned from each one, and the limitations. We start with X-ray diffraction by powders and single crystals. Single crystal X-ray diffraction is used to determine atomic positions precisely and therefore the bond lengths (to a few tens of picometres*) and bond angles of molecules within the unit cell. It gives an overall, average picture of a long-range ordered structure, but is less suited to giving information on the structural positions of defects, dopants, and non-stoichiometric regions. It is often very difficult to grow single crystals, but most solids can be made as a crystalline powder. Powder X-ray diffraction is probably the most commonly employed technique in solid state inorganic chemistry and has many uses from analysis and assessing phase purity to determining structure. Single crystal X-ray diffraction techniques have provided us with the structures upon which the interpretation of most powder data is based.

2.2 X-RAY DIFFRACTION

2.2.1 GENERATION OF X-RAS

The discovery of X-rays was made by a German physicist, Wilhelm Röntgen, in 1895 for which he was awarded the first Nobel Prize in Physics in 1901. The benefits of his discovery in terms of medical diagnosis and treatment, and in investigating molecular and atomic structure are immeasurable, and yet Röntgen was a man of such integrity that he refused to make any financial gain out of his discovery, believing that scientific research should be made freely available.

An electrically heated filament, usually tungsten, emits electrons, which are accelerated by a high potential difference (20–50 kV) and allowed to strike a metal target or anode which is water cooled (Figure 2.1 (a)). The anode emits a continuous spectrum of 'white' X-radiation but superimposed on this are sharp, intense X-ray

* Many crystallographers still work in Ångstroms, Å; 1 Å=100 pm.

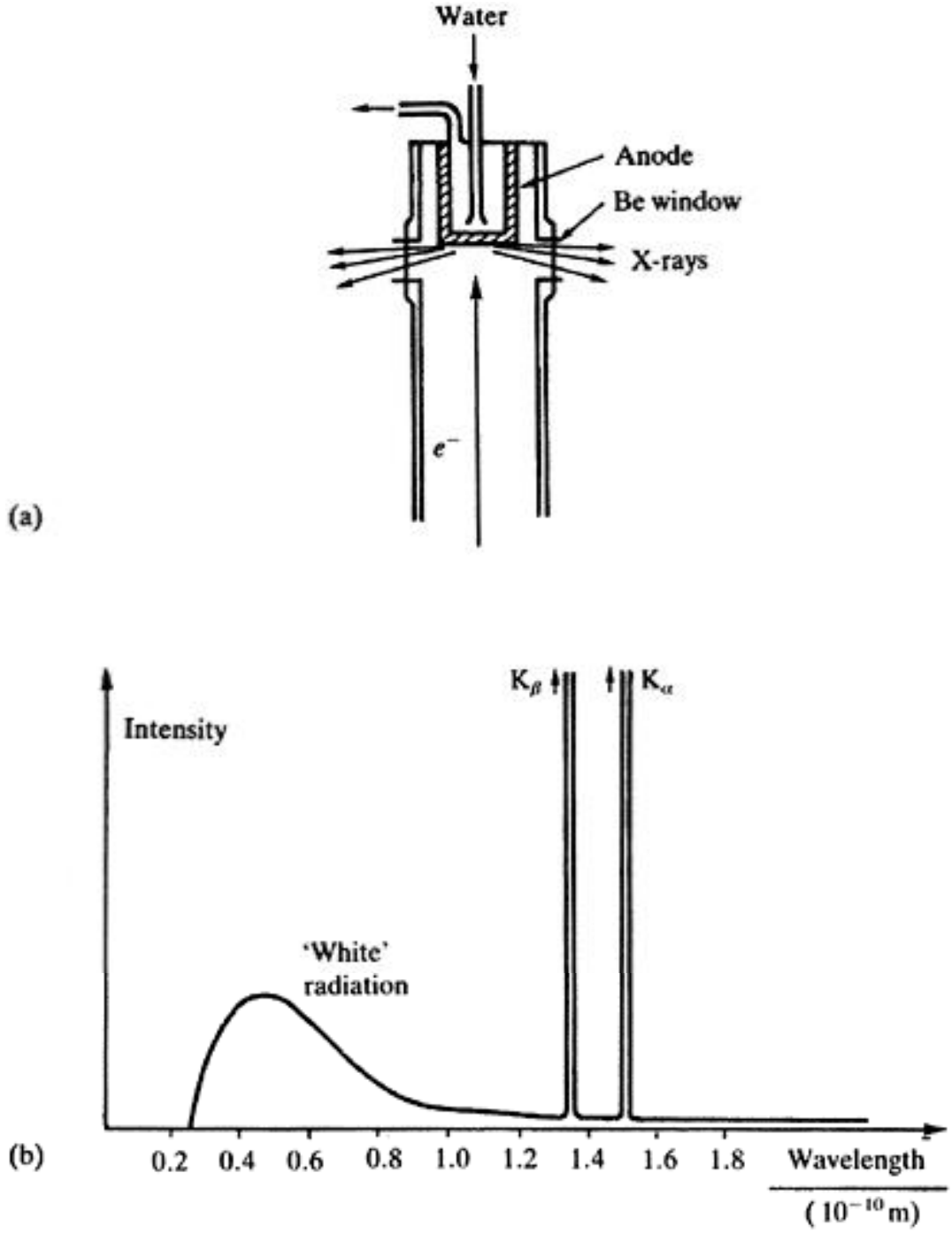

FIGURE 2.1 (a) Section through an X-ray tube; (b) an X-ray emission spectrum.

peaks (K_α, K_β) as depicted in Figure 2.1(b). The frequencies of the K_α and K_β lines are characteristic of the anode metal; the target metals most commonly used in X-ray crystallographic studies are copper and molybdenum, which have K_α lines at 154.18 pm and 71.07 pm, respectively. These lines occur because the bombarding electrons knock out electrons from the innermost K shell (n=1) and this in turn creates vacancies which are filled by electrons descending from the shells above. The decrease in energy appears

as radiation; electrons descending from the L shell (n=2) give the K_α lines and electrons from the M shell (n=3) give the Kβ lines. (These lines are actually very closely spaced doublets—$K_{\alpha 1}$, $K_{\alpha 2}$ and $K_{\beta 1}$, $K_{\beta 2}$—which are usually not resolved.) As the atomic number, Z, of the target increases, the lines shift to shorter wavelength.

Normally in X-ray diffraction, monochromatic radiation (single wavelength or a very narrow range of wavelengths) is required. Usually the K_α line is selected and the K_β line is filtered out by using a filter made of a thin metal foil of the element adjacent (Z−1) in the Periodic Table; thus, nickel effectively filters out the K_β line of copper, and niobium is used for molybdenum. A monochromatic beam of X-rays can also be selected by reflecting the beam from a plane of a single crystal, normally graphite (the reasons why this works will become obvious after you have read the next section).

2.2.2 DIFFRACTION OF X-RAYS

By 1912, the nature of X-rays—whether they were particles or waves—was still unresolved; a demonstration of X-ray diffraction effects was needed to demonstrate their wave nature. This was eventually achieved by Max von Laue using a crystal of copper sulfate as the diffraction grating, work which earned him the Nobel Prize for Physics in 1914. Crystalline solids consist of regular arrays of atoms, ions or molecules with interatomic spacings of the order of 100 pm. For diffraction to take place, the wavelength of the incident light has to be of the same order of magnitude as the spacings of the grating. Because of the periodic nature of the internal structure, it is possible for crystals to act as a three-dimensional diffraction grating to light of a suitable wavelength: a Laue photograph is pictured in Figure 2.2.

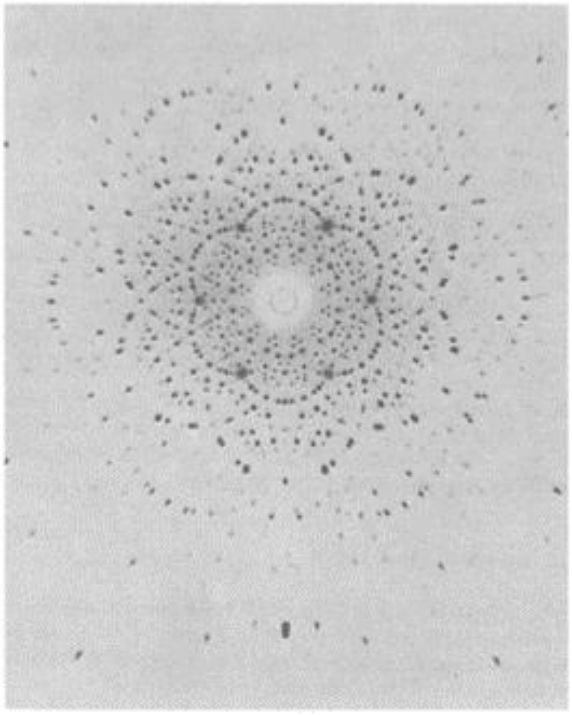

FIGURE 2.2 X-ray diffraction by a crystal of beryl using the Laue method.

(From W.J.Moore (1972) *Physical Chemistry,* 5th edn, Longman, London.)

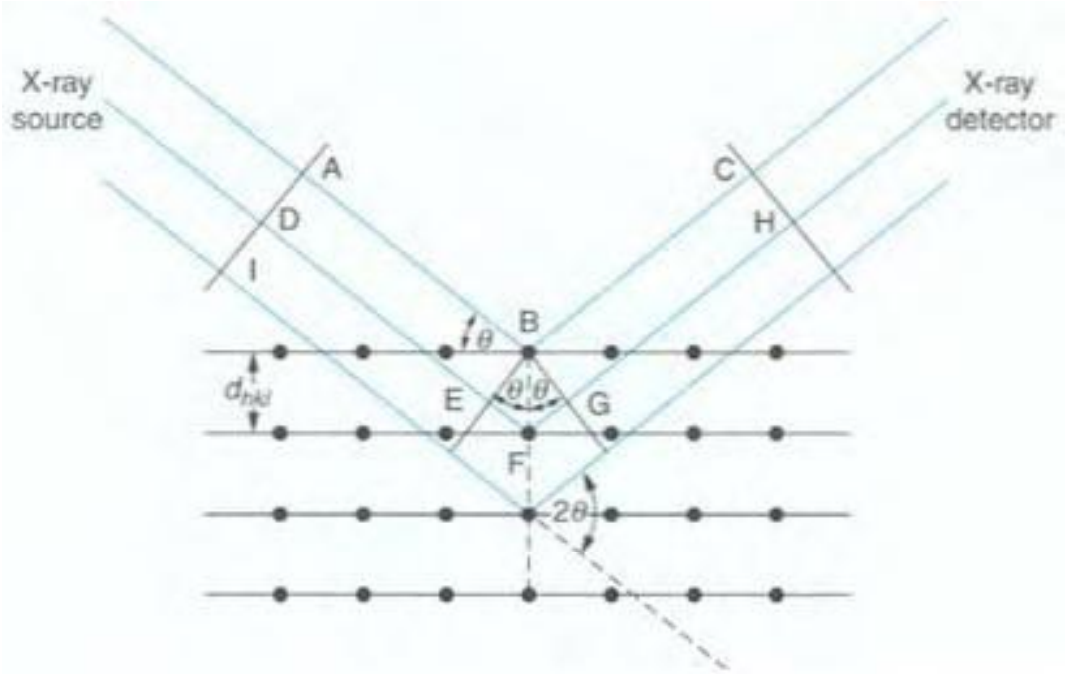

FIGURE 2.3 Bragg reflection from a set of crystal planes with a spacing d_{hkl}.

This discovery was immediately noted by W.H. and W.L.Bragg (father and son), and they started experiments on using X-ray crystal diffraction as a means of structure determination. In 1913 they first determined the crystal structure of NaCl, and they went on to determine many structures including those of KCl, ZnS, CaF_2, $CaCO_3$, and diamond. W.L.(Lawrence) Bragg noted that X-ray diffraction behaves like 'reflection' from the planes of atoms within the crystal and that only at specific orientations of the crystal with respect to the source and detector are X-rays 'reflected' from the planes. It is not like the reflection of light from a mirror, as this requires that the angle of incidence equals the angle of reflection, and this is possible for all angles. With X-ray diffraction, the reflection only occurs when the conditions for constructive interference are fulfilled.

Figure 2.3 illustrates the Bragg condition for the reflection of X-rays by a crystal. The array of black points in the diagram represents a section through a crystal and the lines joining the dots mark a set of parallel planes with Miller indices *hkl* and interplanar spacing d_{hkl}. A parallel beam of monochromatic X-rays ADI is incident to the planes at an angle θ_{hkl}. The ray A is scattered by the atom at B and the ray D is scattered by the atom at F. For the reflected beams to emerge as a single beam of reasonable intensity, they must reinforce, or arrive in phase with one another. This is known as constructive interference, and for constructive interference to take place, the path lengths of the interfering beams must differ by an integral number of wavelengths. If BE and BG are drawn at right angles to the beam, the difference in path length between the two beams is given by:

difference in path length=EF+FG

but

EF=FG=$d_{hkl}\sin\theta_{hkl}$

so

difference in path length=$2d_{hkl}\sin\theta_{hkl}$ (2.1)

This must be equal to an integral number, n, of wavelengths. If the wavelength of the X-rays is λ, then

$n\lambda=2d_{hkl}\sin\theta_{hkl}$ (2.2)

This is known as the **Bragg equation**, and it relates the spacing between the crystal planes, d_{hkl}, to the particular Bragg angle, θ_{hkl} at which reflections from these planes are observed (mostly the subscript hkl is dropped from the Bragg angle θ without any ambiguity as the angle is unique for each set of planes).

When n=1, the reflections are called first order, and when n=2 the reflections are second order and so on. However, the Bragg equation for a second order reflection from a set of planes hkl is

$2\lambda=2d_{hkl}\sin\theta$

which can be rewritten as

$$\lambda = 2\ \frac{d_{hkl}}{2}\sin\theta \qquad (2.3)$$

Equation 2.3 represents a first order reflection from a set of planes with interplanar spacing $\frac{d_{hkl}}{2}$. The set of planes with interplanar spacing $\frac{d_{hkl}}{2}$ has Miller indices $2h\ 2k\ 2l$. Therefore, the second order reflection from hkl is indistinguishable from the first order reflection from $2h\ 2k\ 2l$, and the Bragg equation may be written more simply as

$\lambda=2d_{hkl}\sin\theta$ (2.4)

2.3 POWDER DIFFRACTION

2.3.1 POWDER DIFFRACTION PATTERNS

A finely ground crystalline powder contains a very large number of small crystals, known as crystallites, which are oriented randomly to one another. If such a sample is placed in the path of a monochromatic X-ray beam, diffraction will occur from planes in those crystallites which happen to be oriented at the correct angle to fulfill the Bragg condition.

The diffracted beams make an angle of 2θ with the incident beam. Because the crystallites can lie in all directions while still maintaining the Bragg condition, the reflections lie on the surface of cones whose *semi*-apex angles

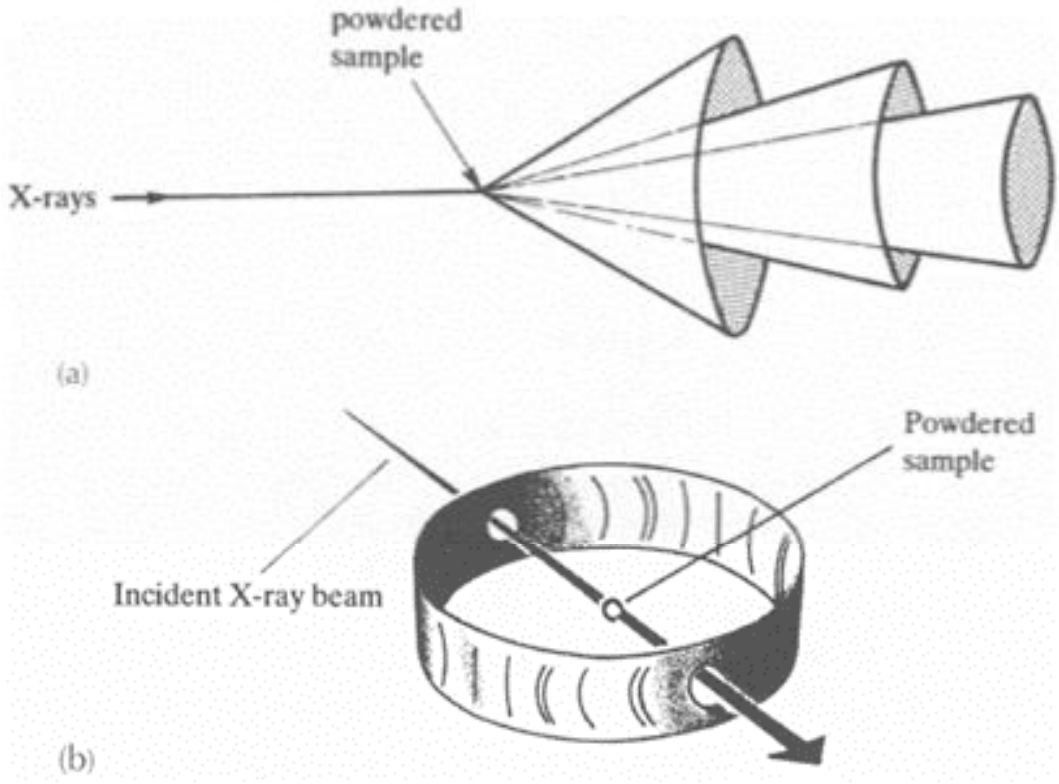

FIGURE 2.4 (a) Cones produced by a powder diffraction experiment; (b) experimental arrangement for a Debye-Scherrer photograph.

are equal to the deflection angle 2θ (Figure 2.4(a)). In the **Debye-Scherrer** photographic method, a strip of film was wrapped around the inside of a X-ray camera (Figure 2.4(b)) with a hole to allow in the collimated incident beam and a beamstop to absorb the undiffracted beam. The sample was rotated to bring as many planes as possible into the diffracting condition, and the cones were recorded as arcs on the film. Using the radius of the camera and the distance along the film from the centre, the Bragg angle 2θ, and thus the d_{hkl} spacing for each reflection can be calculated. Collection of powder diffraction patterns is now almost always performed by automatic diffractometers (Figure 2.5(a)), using a scintillation or CCD detector to record the angle and the intensity of the diffracted beams, which are plotted as intensity against 2θ (Figure 2.5(b)). The resolution obtained using a diffractometer is better than photography as the sample acts like a mirror helping to refocus the X-ray beam. The data, both position and intensity, are readily measured and stored on a computer for analysis.

The difficulty in the powder method lies in deciding which planes are responsible for each reflection; this is known as 'indexing the reflections' (i.e., assigning the correct *hkl* index to each reflection). Although this is often possible for simple compounds in high

symmetry systems, as we shall explain in Section 2.4.3, it is extremely difficult to do for many larger and/or less symmetrical systems.

2.3.2 ABSENCES DUE TO LATTICE CENTRING

First, consider a primitive cubic system. From equation 2.4, we see that the planes giving rise to the reflection with the smallest Bragg angle will have the largest d_{hkl} spacing. In the primitive cubic system the *100* planes have the largest separation

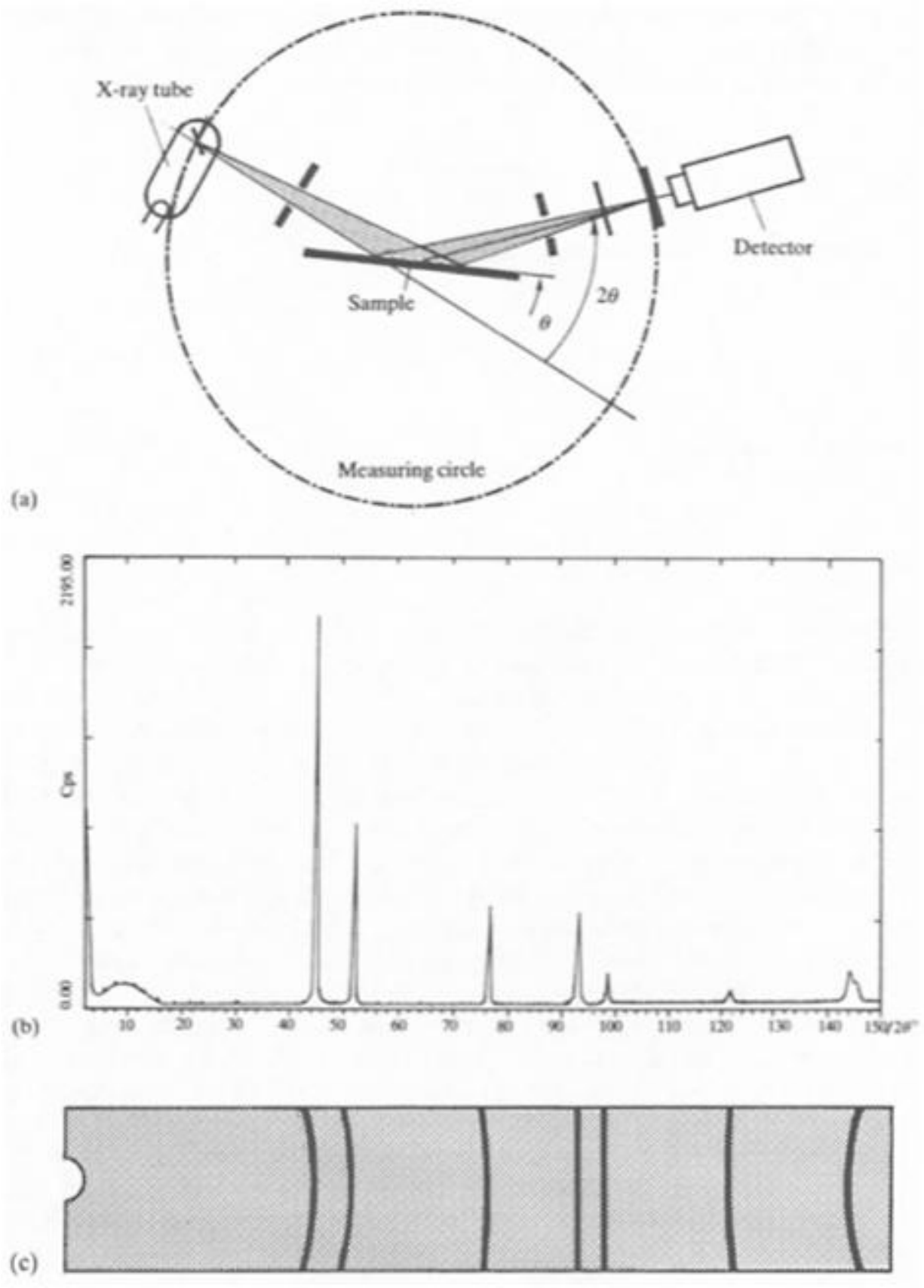

FIGURE 2.5 (a) Diagram of a powder diffractometer; (b) a powder

diffraction pattern for Ni powder compared with (c) the Debye-Scherrer photograph of Ni powder.

and thus give rise to this reflection, and as $a=b=c$ in a cubic system the *010* and the *001* also reflect at this position. For the cubic system, with a unit cell dimension *a,* the spacing of the reflecting planes is given by Equation 2.4

$$d_{hkl} = \frac{a}{\sqrt{(h^2 + k^2 + l^2)}} \tag{2.4}$$

Combining this with the Bragg equation gives

$$\lambda = \frac{2a\sin\theta_{hkl}}{\sqrt{(h^2 + k^2 + l^2)}}$$

and rearranging gives

$$\sin^2\theta_{hkl} = \frac{\lambda^2}{4a^2}(h^2 + k^2 + l^2) \tag{2.5}$$

For the primitive cubic class all integral values of the indices *h, k,* and *l* are possible. Table 2.1 lists the values of *hkl* in order of increasing value of $(h^2+k^2+l^2)$ and therefore of increasing sinθ values.

One value in the sequence, 7, is missing because no possible integral values exists for $(h^2+k^2+l^2)=7$. Other higher missing values exist where $(h^2+k^2+l^2)$ cannot be an integer: 15, 23, 28, etc., but note that this is only an arithmetical phenomenon and is nothing to do with the structure.

Taking Equation 2.5, if we plot the intensity of diffraction of the powder pattern of a primitive cubic system against $\sin^2\theta_{hkl}$ we would get six equi-spaced lines with the 7th, 15th, 23rd, etc., missing. Consequently, it is easy to identify a primitive cubic system and by inspection to assign indices to each of the reflections.

The cubic unit cell dimension *a* can be determined from any of the indexed reflections using Equation 2.5. The experimental error in measuring the Bragg angle is constant for all angles, so to minimize error, either, the reflection with the largest Bragg angle is chosen, or more usually, a least squares refinement to all the data is used.

The pattern of observed lines for the two other cubic crystal systems, body-centred and face-centred is rather different from that of the primitive system. The differences arise because the centring leads to destructive interference for some reflections and these extra missing reflections are known as **systematic absences**.

TABLE 2.1 Values of $(h^2+k^2+l^2)$

hkl	*100*	*110*	*111*	*200*	*210*	*211*	*220*	*300=221*
$(h^2+k^2+l^2)$	1	2	3	4	5	6	8	9

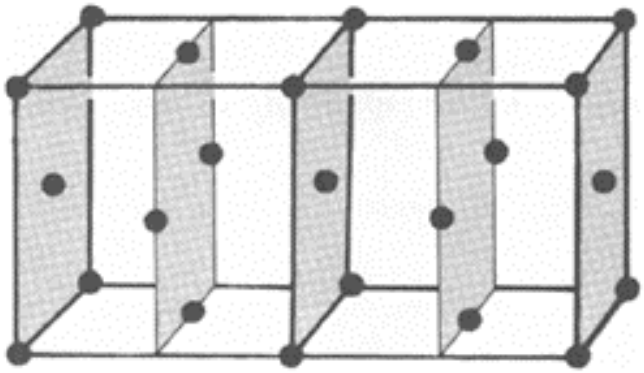

FIGURE 2.6 Two F-centred unit cells with the *200* planes shaded.

Consider the *200* planes that are shaded in the F face-centred cubic unit cells depicted in Figure 2.6; if *a* is the cell dimension, they have a spacing $\frac{a}{2}$. Figure 2.7 illustrates the reflections from four consecutive planes in this structure. The reflection from the *200* planes is exactly out of phase with the *100* reflection. Throughout the crystal, equal numbers of the two types of planes exist, with the result that complete destructive interference occurs and no *100* reflection is observed. Examining reflections from all the planes for the F face-centred system in this way, we find that in order for a reflection to be observed, the indices must be either *all odd* or *all even*.

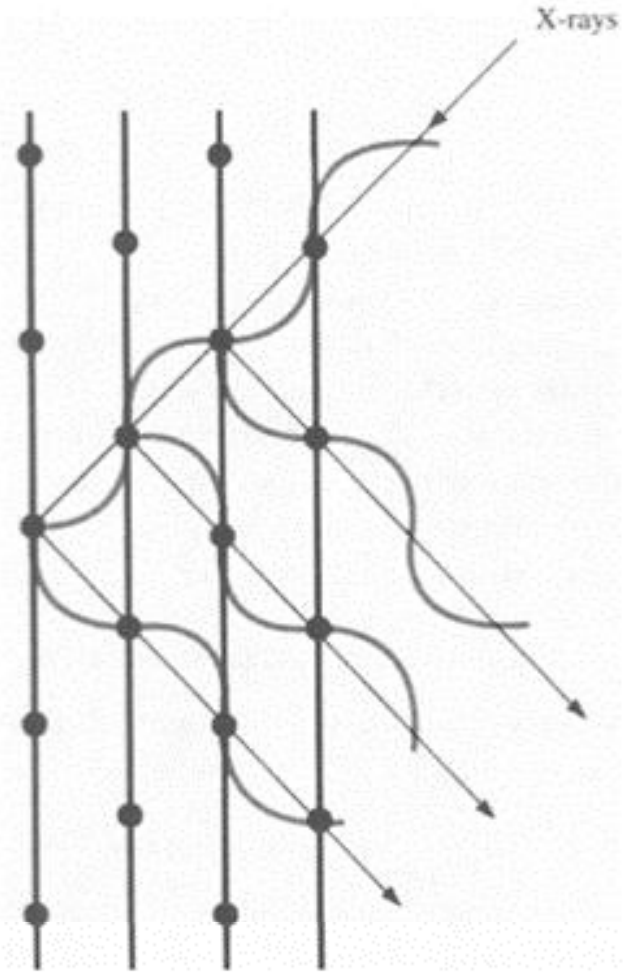

FIGURE 2.7 The *100* reflection from an F-centred cubic lattice.

TABLE 2.2 Allowed values of $(h^2+k^2+l^2)$ for cubic crystals

Forbidden numbers	Primitive, P	Face-centred, F	Body-centred, I	Corresponding *hkl* values
	1			*100*
	2		2	*110*
	3	3		*111*
	4	4	4	*200*
	5			*210*
	6		6	*211*
7				–
	8	8	8	*220*
	9			*221, 300*

	10		10	*310*
	11	11		*311*
	12	12	12	*222*
	13			*320*
	14		14	*321*
15				–
	16	16	16	*400*

A similar procedure for the body-centred cubic system finds that for reflections to be observed the *sum of the indices must be even.*

It is possible to characterize the type of Bravais lattice present by the pattern of systematic absences. Although our discussion has centred on cubic crystals, these absences apply to all crystal systems, not just to cubic, and are summarized in Table 2.3 at the end of the next section. The allowed values of $h^2+k^2+l^2$ are listed in Table 2.2 for each of the cubic lattices.

Using these pieces of information and Equation (2.5), we can see that if the observed $\sin^2\theta$ values for a pattern are in the ratio 1:2:3:4:5:6:8…, then the unit cell is likely to be primitive cubic, and the common factor is $\frac{\lambda^2}{4a^2}$.

A face-centred cubic unit cell can also be recognized: if the first two lines have a common factor, A, then dividing all the observed $\sin^2\theta$ values by A gives a series of numbers, 3, 4, 8, 11, 12, 16…, and A is equal to $\frac{\lambda^2}{4a^2}$.

A body-centred cubic system gives the values of $\sin^2\theta$ in the ratio 1:2:3:4 :5:6:7:8…with the values 7 and 15 apparently *not* missing, but now the common factor is $\frac{2\lambda^2}{4a^2}$.

TABLE 2.3 Systematic absences due to translational symmetry elements

Symmetry element		Affected reflection	Condition for reflection to be present
Primitive lattice	P	*hkl*	None
Body-centred lattice	I	*hkl*	*h+k+l*=even
Face-centred lattice	A	*hkl*	*k+l*=even
	B		*h+l*=even
	C		*h+k*=even
Face-centred lattice	F		*h k l* all odd or all even

twofold screw, 2_1 along			
fourfold screw, 4_2 along	*a*	*h00*	*h*=even
sixfold screw, 6_3 along			
threefold screw, 3_1, 3_2 along		*00l*	*l* divisible by 3
sixfold screw, 6_2, 6_4 along	*c*		
fourfold screw 4_1, 4_3 along	*a*	*h00*	*h* divisible by 4
sixfold screw, 6_1, 6_5 along	*c*	*001*	*l* divisible by 6
Glide plane perpendicular to	*b*		
Translation $\frac{a}{2}$(*a* glide)			*h*=even
Translation $\frac{c}{2}$(*c* glide)		*h0l*	*l*=even
$\frac{b}{2}+\frac{c}{2}$ (*n* glide)			*h+l*=even
$\frac{b}{4}+\frac{c}{4}$(*d* glide) (*d* glide			*h+l* divisible by 4

2.3.3 SYSTEMATIC ABSENCES DUE TO SCREW AXES AND GLIDE PLANES

The presence of translational symmetry elements in a crystal structure can be detected because they each lead to a set of systematic absences in the *hkl* reflections. Figure 1.20 and Figure 1.21 illustrate how a twofold screw (2_1) along *z* introduces a plane of atoms exactly halfway between the *001* planes: reflections from these planes will destructively interfere with reflections from the *001* planes and the *001* reflection will be absent, as will any reflection for which *l* is odd. The effect of a glide plane (Figure 1.19) is to introduce a plane of atoms halfway along the unit cell in the direction of the glide. For an *a* glide perpendicular to *b,* the *10l* reflection will be absent, and in general the *h0l* reflections will only be present when *h* is even. Systematic absences are summarized in Table 2.3.

Fairly powerful computer programmes for indexing are now in existence, and powder diffraction patterns can be indexed readily for the high symmetry crystal classes such as cubic, tetragonal, and hexagonal. For the other systems, the pattern often consists of a large number of overlapping lines, and indexing can be much more difficult or even impossible.

From the cubic unit cell dimension *a,* we can calculate the volume of the unit cell, *V* If the density, ρ, of the crystals are known, then the mass of the contents of the unit cell, *M,* can also be calculated

$$\rho = \frac{M}{V} \qquad (2.6)$$

From a knowledge of the molecular mass, the number of molecules, *Z*, in the unit cell can be calculated. Examples of these calculations are in the questions at the end of the chapter.

The density of crystals can be determined by preparing a mixture of liquids (in which the crystals are insoluble!) such that the crystals neither float nor sink: the crystals then have the same density as the liquid. The density of the liquid can be determined in the traditional way using a density bottle.

2.3.4 USES OF POWDER X-RAY DIFFRACTION

Identification of Unknowns and Phase Purity

Powder diffraction is difficult to use as a method of determining crystal structures for anything other than simple high symmetry crystals because as the structures become more complex the number of lines increases so that overlap becomes a serious problem and it is difficult to index and measure the intensities of the reflections. It is usefully used as a fingerprint method for detecting the presence of a known compound or phase in a product. This is made possible by the existence of a huge library of powder diffraction patterns that is regularly updated, known as the Joint Committee for Powder Diffraction Standards (JCPDS) files, which are available on CD-ROM. When the powder diffraction pattern of your sample has been measured and both the d_{hkl} spacings and intensity of the lines recorded, these can be matched against the patterns of known compounds in the files. With modern diffractometers, the computer matches the recorded pattern of the sample to the patterns stored in the JCPDS files (Figure 2.8).

The identification of compounds using powder diffraction is useful for qualitative analysis, such as mixtures of small crystals in geological samples. It also gives a rough check of the purity of a sample—but note that powder diffraction does not detect amorphous products or impurities of less than about 5%.

Powder diffraction can confirm whether two similar compounds, where one metal substitutes for another for instance, have an isomorphous structure.

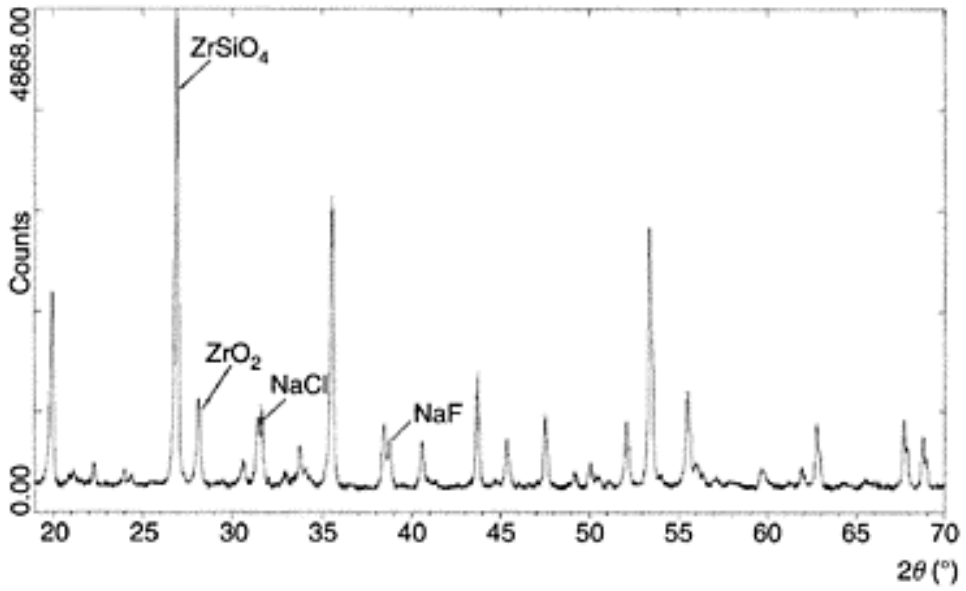

FIGURE 2.8 X-ray diffraction pattern for the preparation of zircon, $ZrSiO_4$, from zirconia, ZrO_2, silica, SiO_2, and sodium halide mineralisers. The peaks demonstrate zircon to be the main product containing traces of all the starting materials.

Crystallite Size

As the crystallite size decreases, the width of the diffraction peak increases. To either side of the Bragg angle, the diffracted beam will destructively interfere and we expect to see a sharp peak. However, the destructive interference is the resultant of the summation of all the diffracted beams, and close to the Bragg angle it takes diffraction from very many planes to produce complete destructive interference. In small crystallites not enough planes exist to produce complete destructive interference, and so we see a broadened peak.

The Debye-Scherrer formula enables the thickness of a crystallite to be calculated from the peak widths:

$$T = \frac{C\lambda}{B\cos\theta} = \frac{C\lambda}{(B_M^{\,2} - B_S^{\,2})^{\frac{1}{2}}\cos\theta} \qquad (2.7)$$

where T is the crystallite thickness, λ the wavelength of the X-rays (T and λ have the same units), θ the Bragg angle, and B is the full-width at half-maximum (FWHM) of the peak (radians) corrected for instrumental broadening. (B_M and B_s are the FWHMs of the sample and of a standard, respectively. A highly crystalline sample with a diffraction peak in a similar position to the sample is chosen and this gives the measure of the broadening due to instrumental effects.)

This method is particularly useful for plate-like crystals with distinctive shear planes (e.g., the *111*) as measuring the peak width of this reflection gives the thickness of the crystallites perpendicular to these planes.

It is a common feature of solid state reactions that reaction mixtures become more crystalline on heating as is evidenced by the X-ray diffraction pattern becoming sharper.

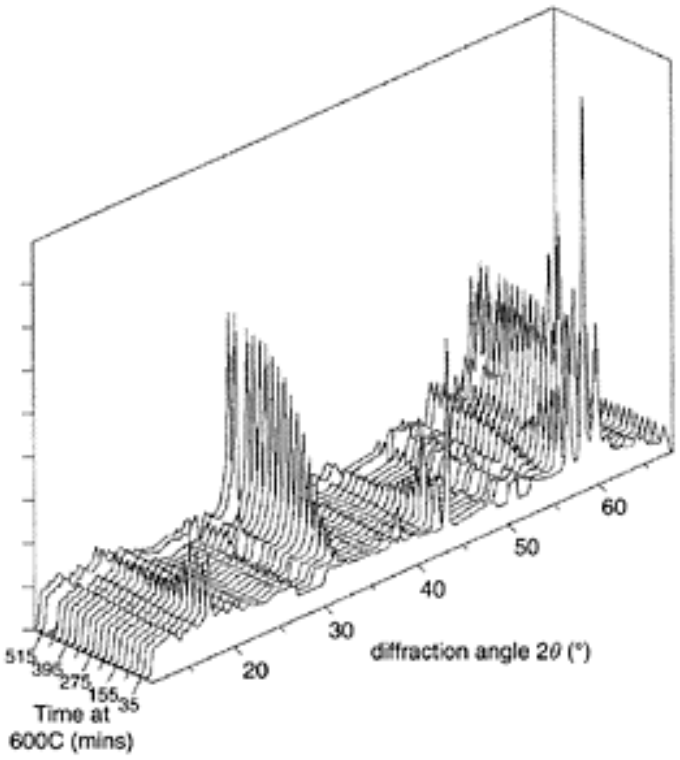

FIGURE 2.9 Powder XRD patterns illustrate the phase changes in ferrosilicon with time, when heated at 600°C. (Courtesy of Professor F.J.Berry, Open University.)

Following Reactions and Phase Diagrams

Powder X-ray diffraction is also a useful method for following the progress of a solid state reaction and determining mechanisms, and for determining phase diagrams. By collecting an X-ray pattern at regular intervals as the sample is heated on a special stage in the diffractometer, evolving phases can be seen as new lines which appear in the pattern, with a corresponding decrease in the lines due to the starting material(s). Figure 2.9 follows the phase transition of ferrosilicon from the non-stoichiometric alpha phase (Fe_xSi_2, x=0.77–0.87) to the stoichiometric beta phase $FeSi_2$, when it is held at 600°C for a specific period. In Figure 2.10, we see three powder diffraction patterns taken at different temperatures from a solid state preparation of an Fe-doped zircon from powdered zirconia and silica according to the equation: $ZrO_2+SiO_2=ZrSiO_4$. Sodium halides are used to bring the reaction temperature down, and ferrrous sulfate was the

source of iron; as the temperature of the reaction mixture is increased, the peaks due to zirconia and silica decrease while those of zircon increase, until at 1060°C, this is the major component. During the reaction, peaks due to intermediates such as Na_2SO_4 and Fe_2O_3 also evolve.

A careful comparison of the intensities of particular lines using standards, not only enable the different phases be identified but also the proportions of different phases to be determined so that a phase diagram can be constructed.

The Rietveld Method

In a high symmetry crystal system, very few peaks occur in the powder pattern, and they are often well resolved and well separated. It is then possible to measure their position and intensity with accuracy, and by the methods we described earlier, index

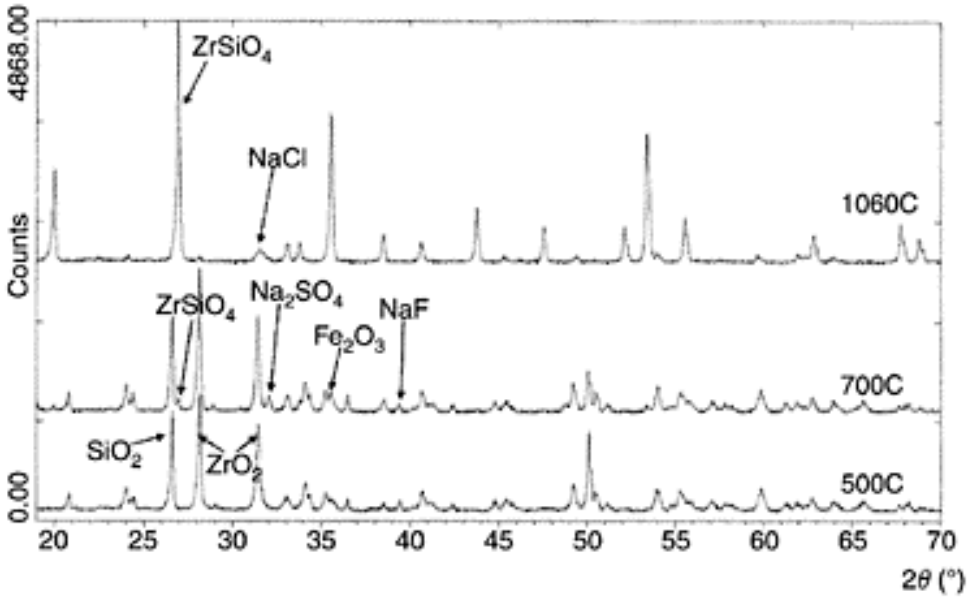

FIGURE 2.10 The phase evolution of iron-doped zircon, $ZrSiO_4$, from zirconia, ZrO_2, silica, SiO_2, ferrous sulphate, $FeSO_4$, and sodium halide mineralisers.

the reflections and solve the structure. For larger and less symmetrical structures, far more reflections overlap considerably, and it becomes impossible to measure the intensities of individual peaks with any accuracy.

A method known as **Rietveld analysis** has been developed for solving crystal structures from powder diffraction data. The Rietveld method involves an interpretation of not only the line position but also of the line intensities, and because there is so much overlap of the reflections in the powder patterns, the method developed by Rietveld involves analysing the overall line profiles. Rietveld formulated a method of assigning each peak a gaussian shape and then allowing the gaussians to overlap so that an overall

line profile could be calculated. The method was originally developed for neutron diffraction. In favourable cases, the Rietveld method can be used to solve a structure from the powder diffraction data. It starts by taking a trial structure, calculating a powder diffraction profile from it and then comparing it with the measured profile. The trial structure can then be gradually modified by changing the atomic positions and refined until a best-fit match with the measured pattern is obtained. The validity of the structure obtained is assessed by an *R* factor, and by a difference plot of the two patterns (which should be a flat line). The method tends to work best if a good trial structure is already known, for instance if the unknown structure is a slight modification of a known structure, with perhaps one metal changed for another (Figure 2.11).

2.4 SINGLE CRYSTAL X-RAY DIFFRACTION

From a single crystal, it is possible to measure the position and intensity of the *hkl* reflections accurately and from this data determine not only the unit cell dimensions and space group, but also the precise atomic positions. In most cases, this can be done with speed and accuracy, and it is one of the most powerful structural techniques available to a chemist.

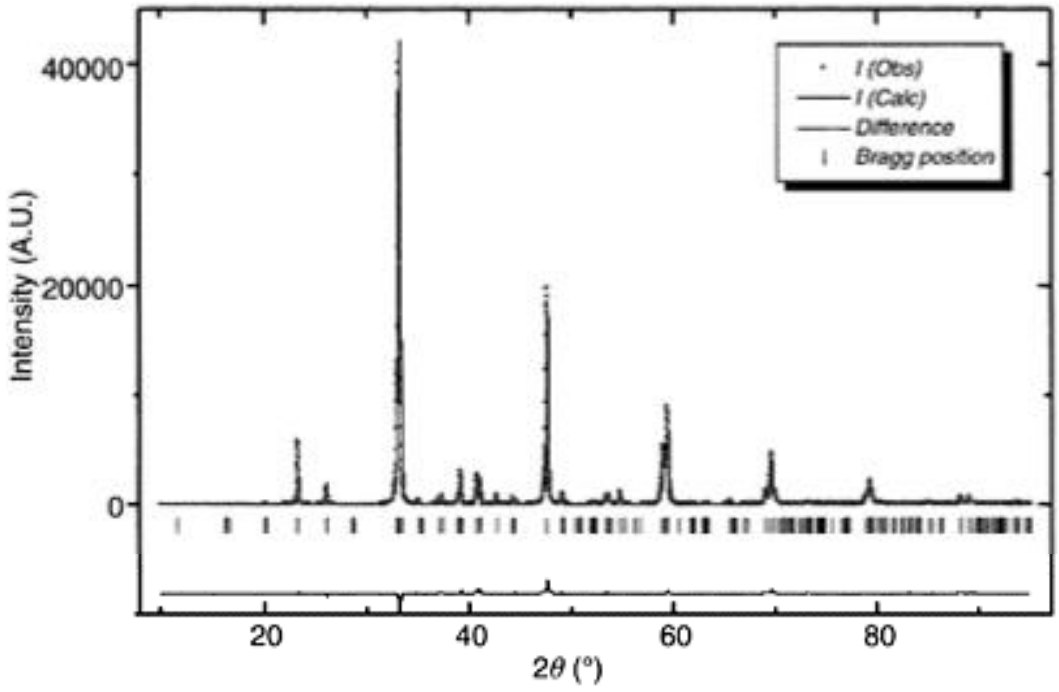

FIGURE 2.11 Rietveld analysis of perovskite with partial substitution of Ti with Ca. (Courtesy of the Royal Society of Chemistry.)

2.4.1 THE IMPORTANCE OF INTENSITIES

So far, we have only discussed the effects of using crystals as three-dimensional diffraction gratings for X-rays. But you may have wondered why one goes to all this trouble. If we want to magnify an object to see its structure in more detail, why not use a lens system as in a microscope or a camera? Here a lens system focuses the light that is scattered from an object (which, if left alone, would form a diffraction pattern) and forms an image. Why not use a lens to focus X-rays and avoid all the complications? The problem is that there is no suitable way in which X-rays can be focussed, and so the effect of the lens has to be simulated by a mathematical calculation on the information contained in the diffracted beams. Much of this information is contained in the intensity of each beam, but as always, there is a snag! The recording methods do not record *all* of the information in the beam because they only record the intensity and are insensitive to the *phase*. Intensity is proportional to the *square* of the amplitude of the wave, and the phase information is lost. Unfortunately, it is this information which derives from the atomic positions in a structure. When a lens focuses light, this information is retained.

So far, we have seen that if we measure the Bragg angle of the reflections and successfully index them, then we get information on the size of the unit cell and, if it possesses any translational symmetry elements, also on the symmetry. In addition, we have seen that the intensity of each reflection is different and this too can be measured. In early photographic work, the relative intensities of the spots on the film were assessed by eye with reference to a standard, and later a scanning microdensitometer was used. In modern diffractometers, the beam is intercepted by a detector, either a charge coupled device (CCD) plate or a scintillation counter, and the intensity of each reflection is recorded electronically.

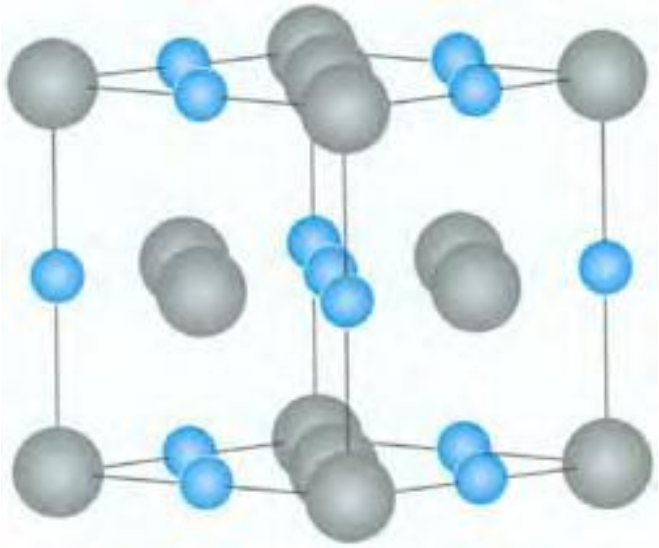

FIGURE 2.12 NaCl unit cell depicting the close-packed *111* and *222* planes.

The interaction which takes place between X-rays and a crystal involves the electrons in the crystal: the more electrons an atom possesses, the more strongly will it scatter the X-

rays. The effectiveness of an atom in scattering X-rays is called the **scattering factor** (or **form factor**), and given the symbol f_0. The scattering factor depends not only on the atomic number, but also on the Bragg angle θ and the wavelength of the X-radiation: as the Bragg angle increases, the scattering power drops off. The decrease in scattering power with angle is due to the finite size of an atom; the electrons are distributed around the nucleus and as θ increases, the X-rays scattered by an electron in one part of the atom are increasingly out of phase with those scattered in a different part of the electron cloud (see Figure 2.13a).

Why are intensities important? A simple example demonstrates this clearly. We know that the heavier an atom is, the better it is at scattering X-rays. On the face of it we might think that the planes containing the heavier atoms will give the more intense reflections. While this is true, the overall picture is more complicated than that because there are interactions with the reflected beams from other planes to take into account, which may produce *destructive interference*. Consider the diffraction patterns produced by NaCl and KCl crystals which both have the same structure (Figure 2.12). The structure can be thought of as two interlocking *ccp* arrays of Na^+ and Cl^- ions. The unit cell depicted in the figure has close-packed layers of Cl^- ions that lie parallel to a body diagonal, with indices *111*. Lying exactly halfway in between the *111* layers, and parallel to them, are close-packed layers of Na^+ ions; this means that a reflection from the Cl^- close-packed layers is exactly out of phase with that from the equivalent Na^+ layers. Because a chloride ion has 18 electrons it scatters the X-rays more strongly than a sodium ion with 10 electrons, the reflections partially cancel and the intensity of the *111* reflection will be weak. The *222* layers contain the close-packed layers of both Na^+ and Cl^-, and this will be a strong reflection because the reflected waves will now reinforce one another. When we come to look at the equivalent situation in KCl, the reflection from the *111* layers containing K^+ ions is exactly out of phase with the reflection from the Cl^- close-packed layers. But, K^+ and Cl^- are isoelectronic, and so their scattering factors for X-rays are virtually identical and the net effect is that the two reflections cancel and the *111* reflection appears to be absent. Similarly, this means that the first observed reflection in the diffraction pattern from KCl is the *200* and it would be very easy to make the mistake that this was the *100* reflection from a primitive cubic cell with a unit cell length half that of the real face-centred cell.

The resultant of the waves scattered by all the atoms in the unit cell, in the direction of the *hkl* reflection, is called the **structure factor,** F_{hkl}, and is dependent on both the position of each atom and its scattering factor. It is given by the general expression for j atoms in a unit cell

$$F_{hkl} = \sum_j f_j e^{2\pi i(hx_j + ky_j + lz_j)} \qquad (2.8)$$

where f_j is the scattering factor of the jth atom and $x_j\ y_j\ z_j$ are its fractional coordinates. Series such as this can also be expressed in terms of sines and cosines, more obviously reflecting the periodic nature of the wave; they are known as **Fourier series**. In a crystal which has a centre of symmetry and n unique atoms in the unit cell (the unique set of atoms is known as the **asymmetric unit**), Equation (2.8) simplifies to

$$F_{hkl} = 2\sum_{n} f_n \cos 2\pi(hx_n + ky_n + lz_n) \qquad (2.9)$$

The electron density distribution within a crystal can be expressed in a similar way as a three-dimensional Fourier series:

$$\rho(x,y,z) = \frac{1}{V}\sum_{h}\sum_{k}\sum_{l} F_{hkl} e^{-2\pi i(hx + ky + lz)} \qquad (2.10)$$

where $\rho(x,y,z)$ is the electron density at a position $x\ y\ z$ in the unit cell and V is the volume of the unit cell. Notice the similarity between the expressions in Equation (2.8) and Equation (2.10). In mathematical terms, the electron density is said to be the **Fourier transform** of the structure factors and vice versa. This relationship means that if the structure factors are known, then it is possible to calculate the electron density distribution in the unit cell, and thus the atomic positions.

The intensity of the *hkl* reflections, I_{hkl}, are measured as described previously and form the data set for a particular crystal. The intensity of a reflection is proportional to the square of the structure factor:

$$I_{hkl} \propto F_{hkl}^2 \qquad (2.11)$$

Taking the square root of the intensity gives a value for the *magnitude* of the structure factor (mathematically this is known as the *modulus* of the structure factor denoted by the vertical bars either side).

$$|F_{hkl}| \propto \sqrt{I_{hkl}} \qquad (2.12)$$

Before this information can be used, the data set has to undergo some routine corrections, this process is known as **data reduction**. The **Lorentz correction,** L, relates to the geometry of the collection mode; the **polarization correction,** p, allows for the fact that the nonpolarized X-ray beam, may become partly polarized on reflection, and an **absorption correction** is often applied to data, particularly for inorganic structures, because the heavier atoms absorb some of the X-ray beam, rather than just scatter it. Corrections can also be made for **anomalous dispersion,** which affects the scattering power of an atom when the wavelength of the incident X-ray is close to its absorption edge. These corrections are applied to the scattering factor, f_0, of the atom.

The structure factor (and thus the intensity of a reflection) is dependent on both the position of each atom and its scattering factor. The structure factor can be *calculated,* therefore, from a knowledge of the types of atoms and their positions using Equation (2.8) or Equation (2.9). It is the great problem of X-ray crystallography that we need to be able to do the reverse of this calculation—we have the measured magnitudes of the structure factors, and from them we want to calculate the atomic positions. But there is the snag, which we mentioned earlier, known as **the phase problem**. When we take the square root of the intensity, we only obtain the modulus of the structure factor, and so we only know its magnitude and not its sign. The phase information is unfortunately lost, and we need it to calculate the electron density distribution and thus the atomic positions.

2.4.2 SOLVING SINGLE CRYSTAL STRUCTURES

It would seem to be an unresolvable problem—to calculate the structure factors we need the atomic positions and to find the atomic positions we need both the amplitude and the phase of the resultant waves, and we only have the amplitude. Fortunately, many scientists over the years have worked at finding ways around this problem, and have been extremely successful, to the extent that for many systems the solving of the structure has become a routine and fast procedure.

Single crystal X-ray diffraction data is nowadays collected using a computer controlled diffractometer, which measures the Bragg angle θ and the intensity I for each *hkl* reflection. Many modern diffractometers employ a flat-plate detector (CCD), so that all the reflections can be collected and measured at the same time. A full data set, which can be thousands of reflections, can be accumulated in hours rather than the days or weeks of earlier times.

To summarize what we know about a structure:

- The size and shape of the unit cell is determined, usually from rotation photographs and scanning routines directly on the diffractometer.
- The reflections are indexed, and from the systematic absences the Bravais lattice and the translational symmetry elements of the structure determined: this information often determines the space group unequivocally, or narrows the possibilities down to a choice of two or three.
- The intensities of the indexed reflections are measured and stored as a data file.
- Correction factors are applied to the raw intensity data.
- Finally, the square roots of the corrected data are taken to give a set of observed structure factors. These are known as F_{obs} or F_o.
- To calculate the electron density distribution in the unit cell, we need to know not only the magnitudes of the structure factors, but also their phase.

Crystal structures are solved by creating a set of trial phases for the structure factors. Two main methods are used to do this. The first is known as the **Patterson** method, and it relies on the presence of at least one (but not many) heavy atoms in the unit cell and so is useful for solving many inorganic molecular structures. The second is called **direct methods,** and it is best used for structures where the atoms have similar scattering properties. Direct methods calculate mathematical probabilities for the phase values and hence an electron density map of the unit cell; theoreticians have produced packages of accessible computer programs for solving and refining structures.

Once the atoms in a structure have been located, a calculated set of structure factors, F_{calc} or F_c is determined for comparison with the F_{obs} magnitudes, and the positions of the atoms are refined using **least-squares methods,** for which standard computer programs are available. In practice, atoms vibrate about their equilibrium positions; this is often called **thermal motion,** although it depends not only on the temperature, but also on the mass of the atom and the strengths of the bonds holding it. The higher the temperature, the bigger the amplitude of vibration and the electron density becomes spread out over a larger volume, thus causing the scattering power of the atom to fall off more quickly. Part of the refinement procedure is to allow the electron density of each atom to refine in a sphere around the nucleus. Structure determinations usually quote an adjustable parameter known as the **isotropic displacement parameter,** B (also called the

isotropic temperature factor). The electron density of each atom can also be refined within an ellipsoid around its nucleus, when an **anisotropic displacement parameter** correction is applied which has six adjustable parameters.

The residual index, or ***R* factor,** gives a measure of the difference between the observed and calculated structure factors and therefore of how well the structure has refined. It is defined as

$$R = \frac{\sum |(|F_o| - |F_c|)|}{\sum |F_o|} \qquad (2.13)$$

and is used to give a guide to the correctness and precision of a structure. In general, the lower the *R* value, the better the structure determination. *R* values have to be used with caution because it is not unknown for structures to have a low *R* value and still be wrong, although fortunately this does not happen often. No hard and fast rules exist for the expected value of *R,* and interpreting them is very much a matter of experience. It is usually taken as a rule of thumb for small molecule structures, that a correct structure for a reasonable quality data set would refine to below an *R* of 0.1, anything above should be viewed with some degree of suspicion. That said, most structures nowadays, if collected from good quality crystals on modern diffractometers, would usually refine to below *R* 0.05 and often to below *R* 0.03.

A good structure determination, as well as having a low *R* value, will also have low standard deviations on both the atomic positions and the bond lengths calculated from these positions. This is probably a more reliable guide to the quality of the refinement.

When a single crystal of a solid can be produced, X-ray diffraction provides an accurate, definitive structure, with bond lengths determined to tenths of a picometre. In recent years, the technique has been transformed from a very slow method reserved only for the most special structures, to a method of almost routine analysis: with modern machines, suites of computer programs and fast computers are used to solve several crystal structures per week.

2.5 NEUTRON DIFFRACTION

The vast majority of crystal structures published in the literature have been solved using X-ray diffraction. However, it is also possible to use neutron diffraction for crystallographic studies. It is a much less commonly used technique because very few sources of neutrons are available, whereas X-ray diffractometers can be housed in any laboratory. It does have advantages for certain structures, however.

The de Broglie relationship states that any beam of moving particles will display wave properties according to the formula

$$\lambda = \frac{h}{\rho} \qquad (2.14)$$

where λ is the wavelength, ρ is the momentum of the particles (ρ=mv, mass× velocity), and h is Planck's constant. Neutrons are released in atomic fission processes from a

uranium target, when they have very high velocities and a very small wavelength. The neutrons generated in a nuclear reactor can be slowed using heavy water so that they have a wavelength of about 100 pm and are thus suitable for structural diffraction experiments. The neutrons generated have a spread of wavelengths, and a monochromatic beam is formed using reflection from a plane of a single-crystal monochromator at a fixed angle (according to Bragg's law). Structural studies need a high flux of neutrons and this usually means that the only appropriate source is a high-flux nuclear reactor such as at Brookhaven and Oak Ridge in the United States, and Grenoble in France.

Alternative spallation sources are also available, such as the Rutherford laboratory in the United Kingdom, where the neutrons are produced by bombarding metal targets with high-energy protons. The diffraction experiments we have seen so far are set up with X-rays of a single wavelength λ, so that in order to collect all the diffracted beams, the Bragg angle θ is varied (Bragg equation $\lambda=2d\sin\theta$). With the spallation source, the whole moderated beam with all its different wavelengths is used at a fixed angle, and the diffraction pattern is recorded as the function of the time of flight of the neutrons. (If we substitute v=D/t [velocity=distance÷time] in the de Broglie relationship, we see that the wavelength of the neutrons is proportional to t: $\lambda = \frac{ht}{Dm}$.) Because this method uses all of the beam, it has the advantage of greater intensity.

The difference between the X-ray and neutron diffraction techniques lies in the scattering process: X-rays are scattered by the electrons around the nucleus, whereas neutrons are scattered by the nucleus. The scattering factor for X-rays increases linearly with the number of electrons in the atom, so that heavy atoms are much more effective at scattering than light atoms. However, because of the size of the atoms relative to the wavelength of the X-rays, the scattering from different parts of the cloud is not always in phase, so the scattering factor decreases with $\sin\theta/\lambda$ due to the destructive interference (Figure 2.13(a)). Because the nucleus is very small, neutron scattering factors do not decrease with $\sin\theta/\lambda$; and because nuclei are similar in size they are all similar in value (hydrogen is anomalously large due to the nuclear spin). Neutron scattering factors are also affected randomly by **resonance scattering,** when the neutron is absorbed by the nucleus and released later. This means that neutron scattering factors cannot be predicted but have to be determined experimentally and they vary for different atoms and indeed for different isotopes (Figure 2.13(b)).

Note that because of the different scattering mechanisms, the bond lengths determined by X-ray and neutron studies will be different. The neutron determination will give the true distance between the nuclei, whereas the X-ray values are distorted by the size of the electron cloud and so are shorter.

2.5.1 USES OF NEUTRON DIFFRACTION

Locating Light Atoms

The fact that neutron scattering factors are similar for all elements means that light atoms scatter neutrons as effectively as heavy atoms and can therefore be located in the crystal structure; for example the X-ray scattering factors for deuterium and tungsten are 1 and 74, respectively, whereas the equivalent neutron values are 0.667 and 0.486. This

property is particularly useful for locating hydrogen atoms in a structure, which can sometimes be difficult to do in an X-ray determination, especially if the hydrogen atoms are in the presence of a heavy metal atom. Accordingly, many neutron studies in the literature have been done with the express purpose of locating hydrogen atoms, or of exploring hydrogen bonding.

Heavy Atoms

The crystals do not absorb neutrons, so they are also useful for studying systems containing heavy atoms that absorb X-rays very strongly.

Similar Atomic Numbers and Isotopes

Atoms near each other in the Periodic Table have very similar X-ray scattering factors and cannot always be distinguished in an X-ray structure determination,

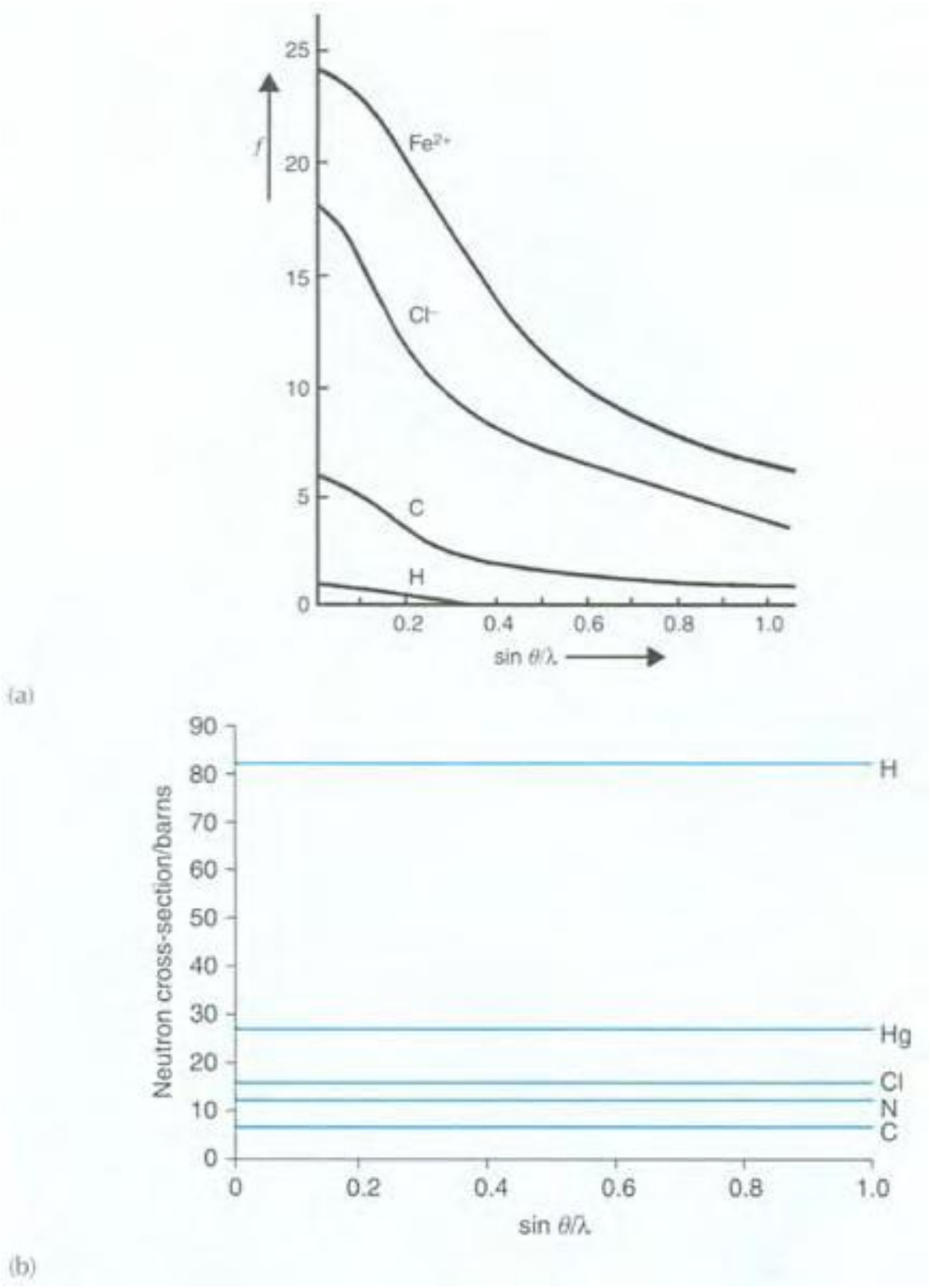

FIGURE 2.13 (a) X-ray scattering factors for hydrogen, carbon, chloride and ferrous ions; (b) the neutron scattering cross sections for several elements, as a function of sinθ/λ.

oxygen and fluorine for instance, or similar metals in an alloy. A neutron structure determination may be able to identify atoms with similar atomic numbers.

Magnetic Properties

As well as the scattering of the neutrons by the nuclei, there is additional magnetic scattering of the neutrons from paramagnetic atoms. This arises because a neutron has spin and so possesses a magnetic moment which can interact with the magnetic moment of an atom. The atomic magnetic moment is due to the alignment of the

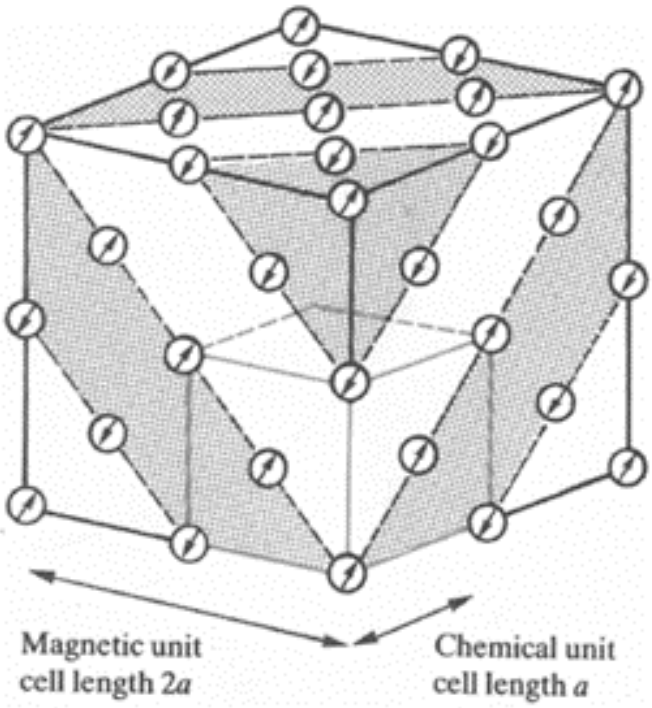

FIGURE 2.14 The magnetic ordering in NiO. The Ni planes only are pictured, and alternate close-packed layers have opposing magnetic moments. Note that the magnetic unit cell length is double that of the normal unit cell.

electron spins, and so this interaction, like the scattering of X-rays, falls off with increasing Bragg angle due to the size of the electron cloud. As will be discussed in Chapter 9, the magnetic moments of a paramagnetic crystal are arranged randomly, but in ferromagnetic, ferrimagnetic, and antiferromagnetic substances the atomic magnetic moments are arranged in an ordered fashion. In ferromagnetic substances, the magnetic moments are arranged so that they all point in the same direction and so reinforce one another; in antiferromagnetic substances, the magnetic moments are ordered so that they completely cancel one another out, and in ferrimagnetic substances the ordering leads to a

partial cancellation of magnetic moments. Magnetic scattering of a polarized beam of neutrons from these ordered magnetic moments gives rise to magnetic Bragg peaks. For instance, the structure of NiO, as determined by X-ray diffraction is the same as NaCl. In the neutron study, however, below 120 K, extra peaks appear due to the magnetic interactions; these give a magnetic unit cell which has a cell length *twice* that of the standard cell. This arises (Figure 2.14) because the alternate close-packed layers of Ni atoms have their magnetic moments aligned in opposing directions, giving rise to antiferromagnetic behaviour.

Rietveld Analysis

The technique of Rietveld profile analysis has already been mentioned in the context of X-ray powder diffraction, but it was with neutron powder diffraction that this technique originated. The fact that the neutron scattering factors are almost invariant with $\sin\theta/\lambda$ means that the intensity of the data does not drop off at high angles of θ as is the case with X-ray patterns, and so a neutron powder pattern tends to yield up considerably more data.

Single Crystal Studies

The flux of a monochromatic source of neutrons is small, and this necessitates the use of large single crystals and long counting times for the experiment, in order to get sufficient intensity. Crystals typically have needed to be at least 1 mm in each direction, and it can be extremely difficult if not impossible to grow such large, perfect crystals. However, new high energy neutron sources are becoming available, such as the one at Grenoble, and the need for these large single crystals in neutron studies is receding.

2.6 ELECTRON MICROSCOPY

Optical microscopy has the advantages of cheapness and ease of sample preparation. A conventional optical microscope uses visible radiation (wavelength 400–700 nm) and so unfortunately cannot resolve images of objects which are smaller than half the wavelength of the light. However, a new technique known as **near-field scanning optical microscopy (NSOM)** uses a sub-wavelength-sized aperture rather than a lens to direct the light on to the sample. Moving the aperture and the sample relative to one another with sub-nanometre precision forms an image, and a spatial resolution of 10 to 100 nm can be achieved. This technique, still in its infancy, has been used successfully to study optical and optoelectronic properties of biological and nanometre scale materials.

Electron microscopy is widely used in the characterization of solids to study structure, morphology, and crystallite size, to examine defects and to determine the distribution of elements. An electron microscope is similar in principle to an optical microscope. The electron beam is produced by heating a tungsten filament, and focused by magnetic fields in a high vacuum (the vacuum prevents interaction of the beam with any extraneous particles in the atmosphere). The very short wavelength of the electrons allows resolution down to 0.1 nm.

2.6.1 SCANNING ELECTRON MICROSCOPY (SEM)

In this technique, the electrons from a finely focused beam are rastered across the surface of the sample. Electrons reflected by the surface of the sample and emitted secondary electrons are detected to give a map of the surface topography of samples such as catalysts, minerals, and polymers. It is useful for looking at particle size, crystal morphology, magnetic domains, and surface defects (Figure 2.15). A wide range of magnification can be used, the best achievable being about 2 nm. The samples may need to be coated with gold or graphite to stop charge building up on the surface.

2.6.2 TRANSMISSION ELECTRON MICROSCOPY (TEM)

In TEM, a thin sample (200 nm) is used and subjected to a high energy, high intensity beam of electrons; those which pass through the sample are detected forming a two-dimensional projection of the sample (Figure 2.16). The electrons may be elastically or inelastically scattered. The instrument can be operated to select either the direct

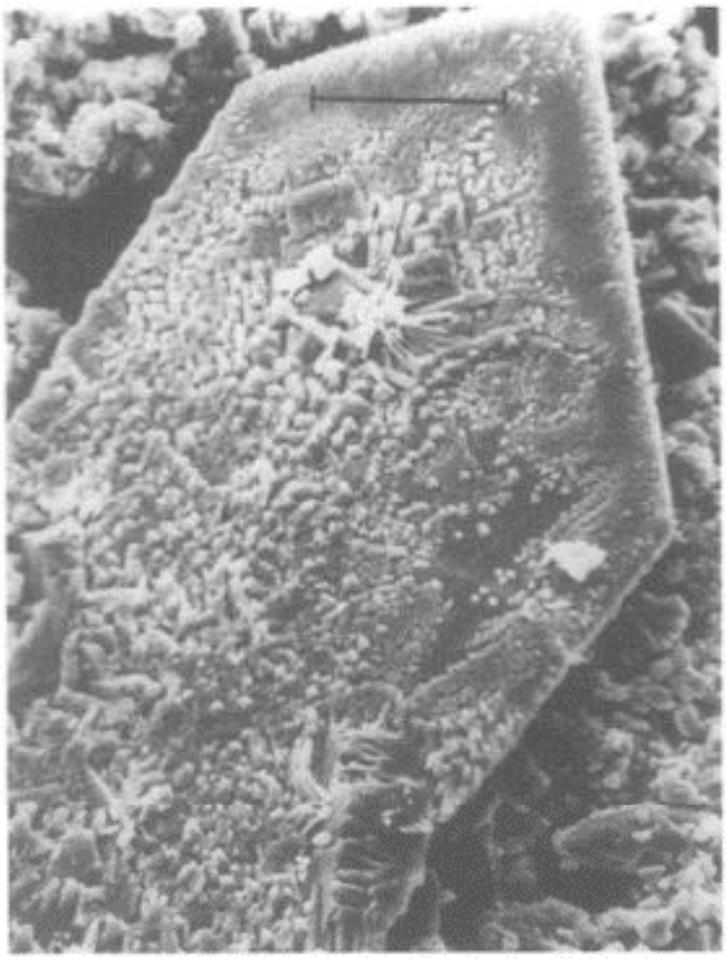

FIGURE 2.15 SEM illustrating crystals of $VSbO_4$ growing out of β-Sb_2O_4 following reaction with V_2O_5.

(Bar=40 μm) (Courtesy of Professor Frank Berry, Open University.)

beam (bright field image) or the diffracted beam (dark field image). In high resolution instruments (sometimes called **high resolution electron microscopy [HREM]**), a very high potential field (up to 10^6 V) accelerates the electrons, increasing their momentum to give very short wavelengths. Because the electrons pass through the sample, TEM/HREM images the bulk structure, and so can detect crystal defects such as phase boundaries, shear planes, and so on (Figure 2.17). Depending on the instrument, resolution of 0.5 nm can be achieved.

2.6.3 SCANNING TRANSMISSION ELECTRON MICROSCOPY (STEM)

These instruments combine the scanning ability of SEM with the high resolution achieved in TEM, a much smaller probe is used (10–15 nm) which scans across the sample.

2.6.4 ENERGY DISPERSIVE X-RAY ANALYSIS (EDAX)

As discussed in Section 2.2.2, an electron beam incident on a metal gives rise to the emission of characteristic X-rays from the metal. In electron microscopy, the elements present in the sample also emit characteristic X-rays. These are separated by a silicon-lithium detector, and each signal collected, amplified and corrected for

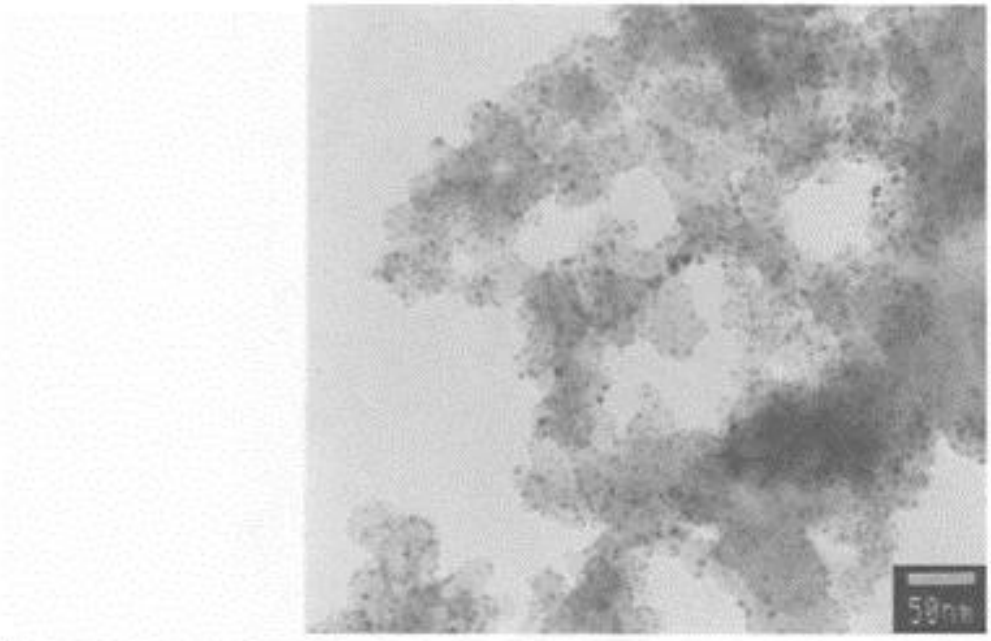

(a)

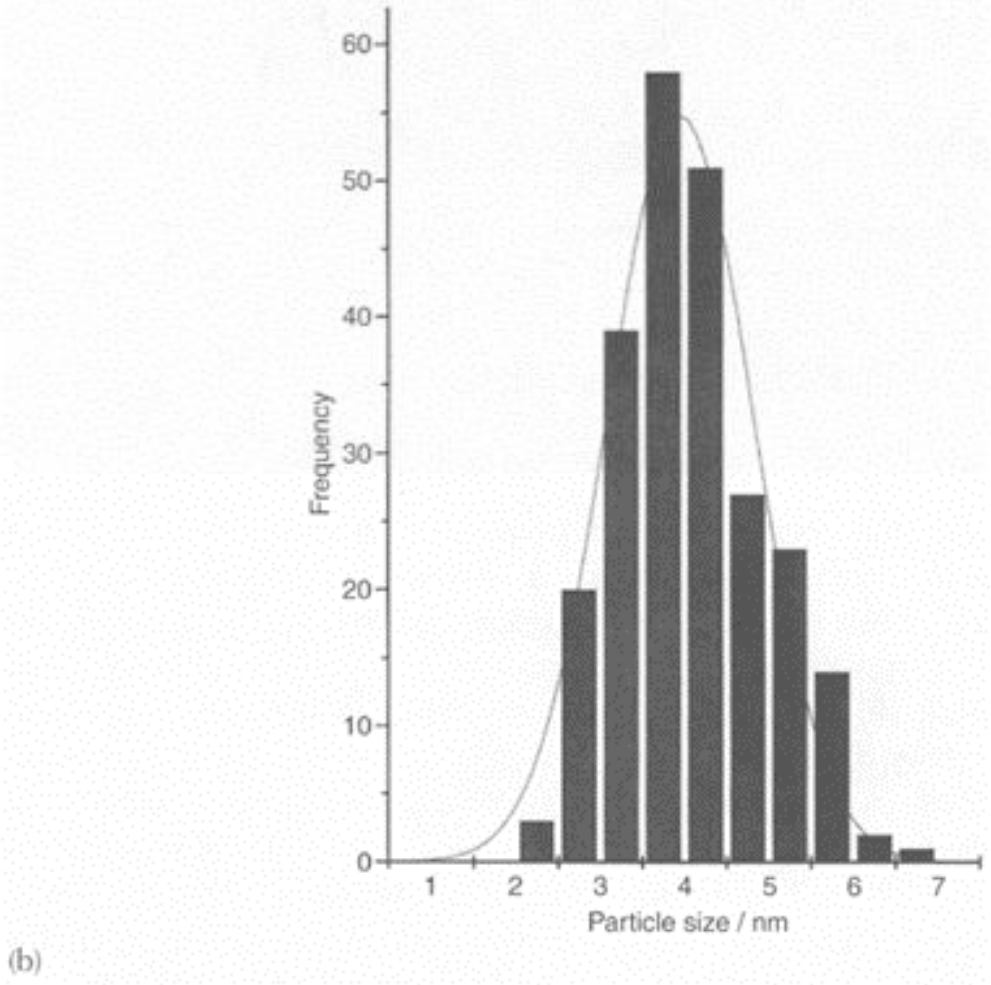

(b)

FIGURE 2.16 (a) TEM image of a supported Pt/Cr bimetallic catalyst on

C; (b) analysis of the metal particle sizes of this catalyst.

absorption and other effects, to give both qualitative and quantitative analysis of the elements present (for elements of atomic number greater than 11) in the irradiated particle, a technique known as **energy dispersive analysis of X-rays (EDAX or EDX)** (Figure 2.18).

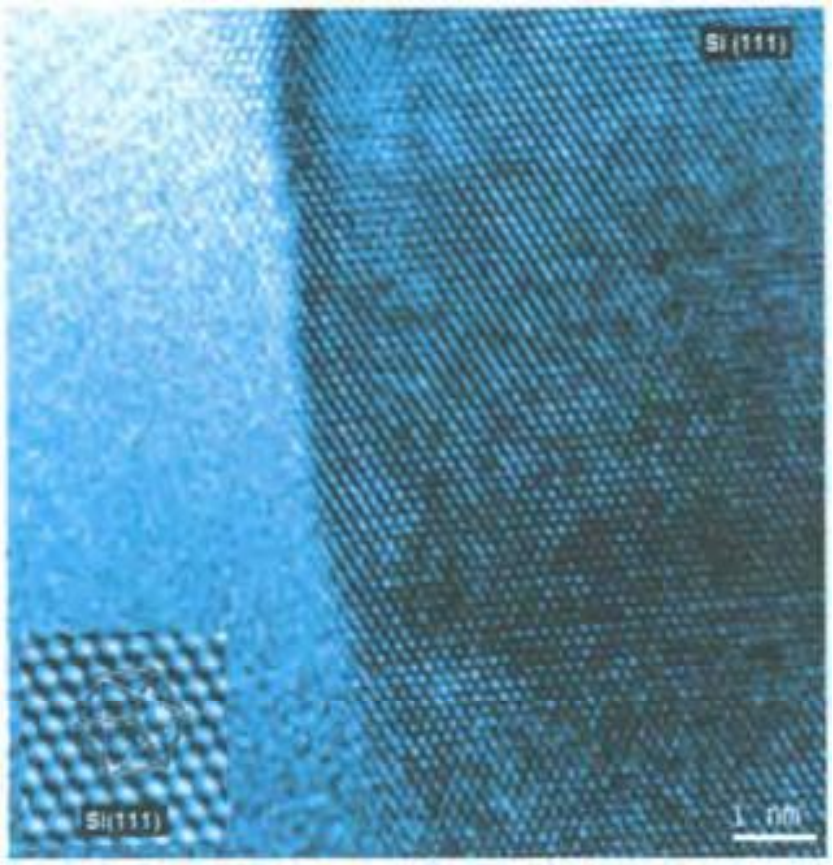

FIGURE 2.17 HREM image showing the atomic sites on the *111* plane of a Si crystal. (Courtesy of Dipl.-Ing. Michael Stöger-Pollach, Vienna University of Technology.)

2.7 X-RAY ABSORPTION SPECTROSCOPY

2.7.1 EXTENDED X-RAY ABSORPTION FINE STRUCTURE (EXAFS)

In high energy accelerators, electrons are injected into an electron storage ring (approximately 30 m in diameter) captured, and accelerated around this circular path by a

series of magnets. When the electrons are accelerated to kinetic energies above the MeV range, they are travelling close to the speed of light and they emit so-called **synchrotron radiation** (Figure 2.19). For an accelerator in the GeV range (the synchrotron at Daresbury, United Kingdom, operates at 2 GeV, and its successor, DIAMOND at the Rutherford Laboratory at 3 GeV) the peak power is radiated at about 10^{18} Hz (approximately 10 keV and 1 Å) in the X-ray region of the electromagnetic spectrum. Unlike X-radiation from a conventional generator, the synchrotron radiation is of uniform intensity across a broad band of wavelengths and several orders of magnitude (10^4–10^6) higher in intensity (Figure 2.20). The shortest X-ray wavelengths emerge as almost fully collimated, polarized beams.

In an EXAFS experiment, the X-radiation is absorbed by a bound electron in a core shell (usually the K shell) and ejected as a photoelectron. If you measure the absorption coefficient of the sample as a function of the X-ray frequency, a sharp rise, or **absorption edge** is observed at the **K** shell threshold energy (Figure 2.21). Each element has its own characteristic **K** shell energy, and this makes it possible to study one type of atom in the presence of many others, by **tuning** the X-ray energy to its absorption edge. The appropriate frequency X-radiation from the continuous synchrotron radiation is selected by using the Bragg reflection from a

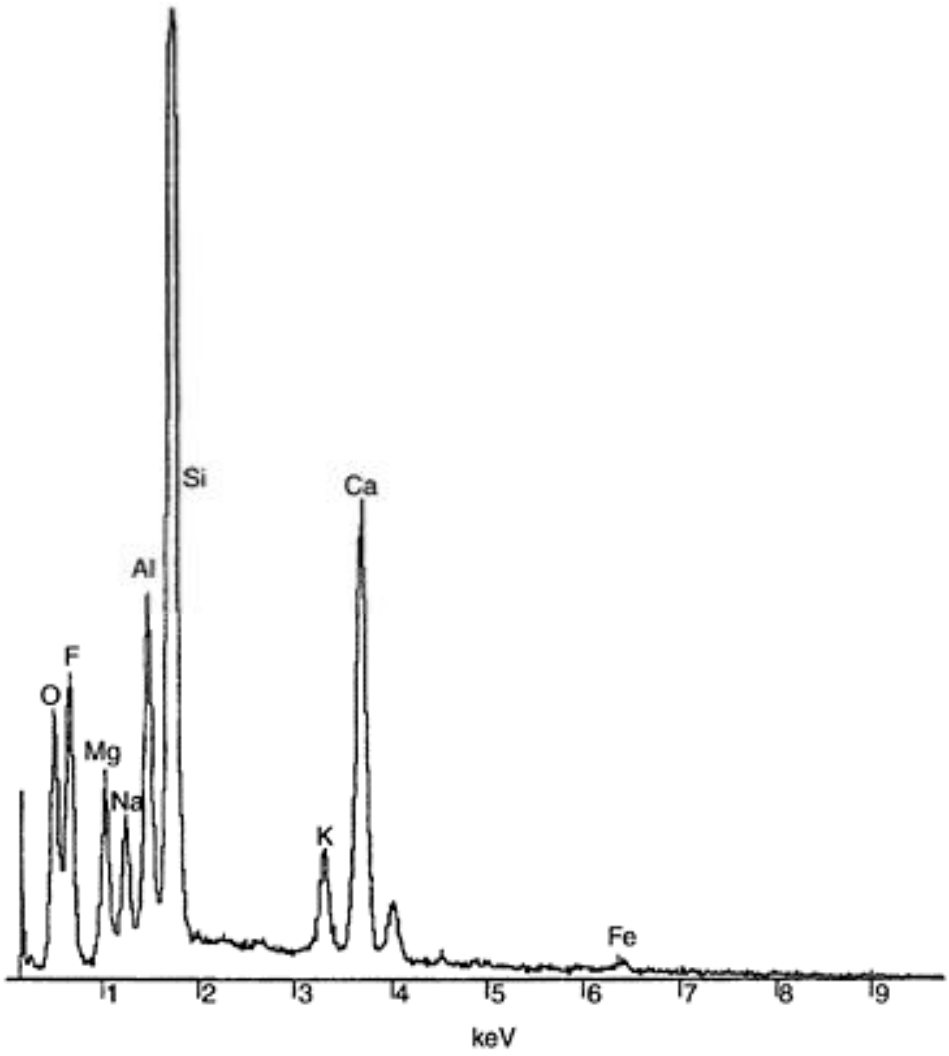

FIGURE 2.18 EDAX analysis of a glaze.

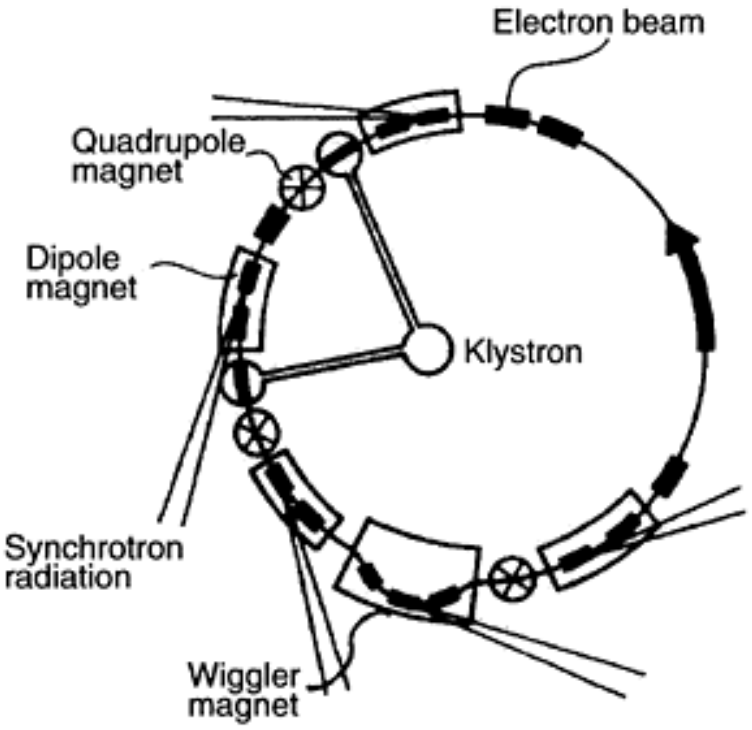

FIGURE 2.19 Diagram of an electron storage ring for producing synchrotron radiation.

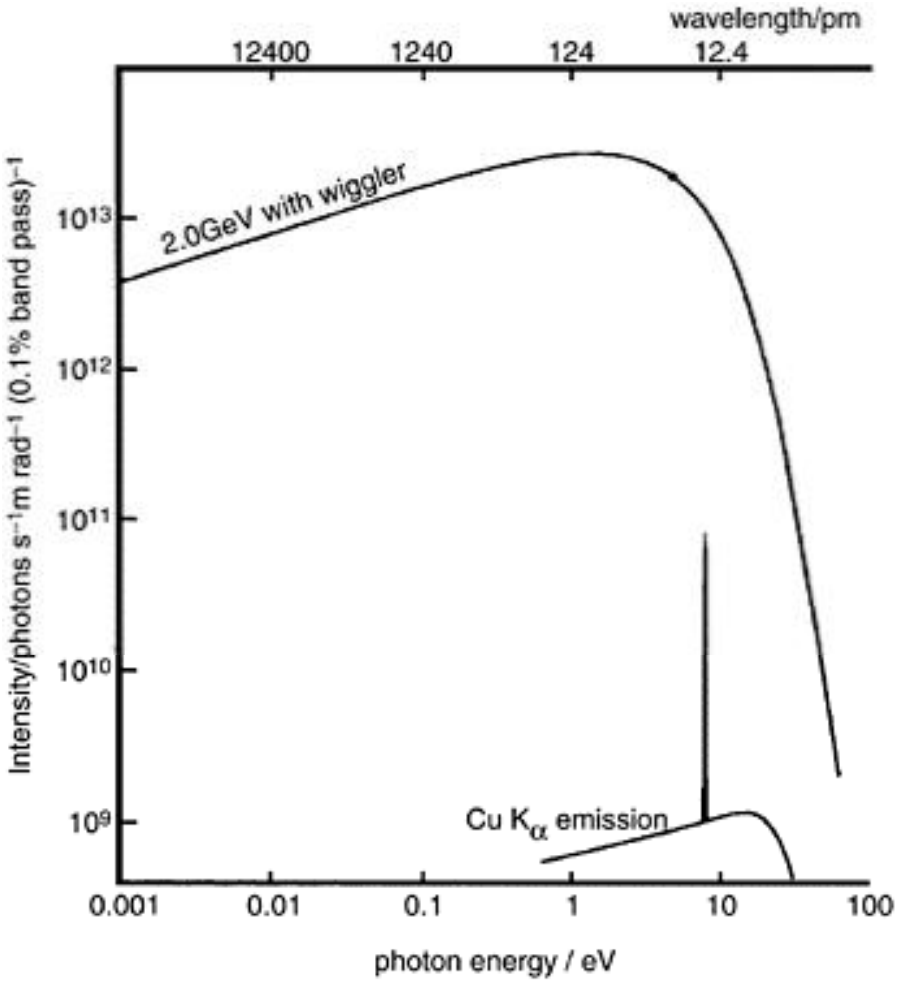

FIGURE 2.20 Synchrotron radiation profile at 2 GeV compared with Cu K_α emission.

single plane of a carefully cut crystal such as Si *(220);* often, two crystals are used, as illustrated in the schematic diagram of a double crystal monochromator in Figure 2.22. By changing the Bragg angle of reflection, the frequency of the X-rays selected may be changed, and thus the absorption edges of a wide range of elements can be studied.

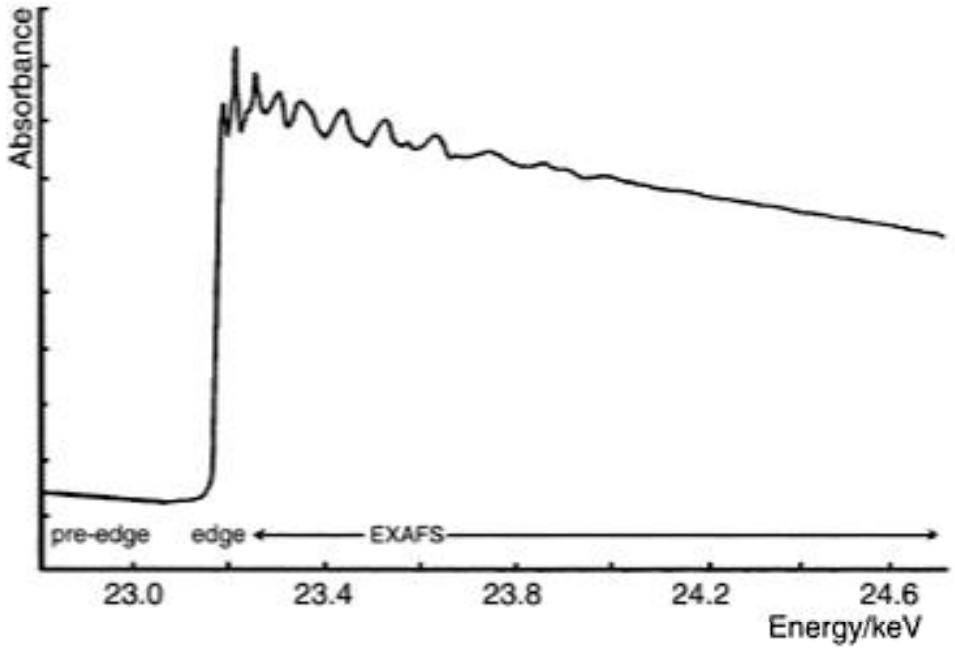

FIGURE 2.21 The Rh absorption edge and EXAFS.

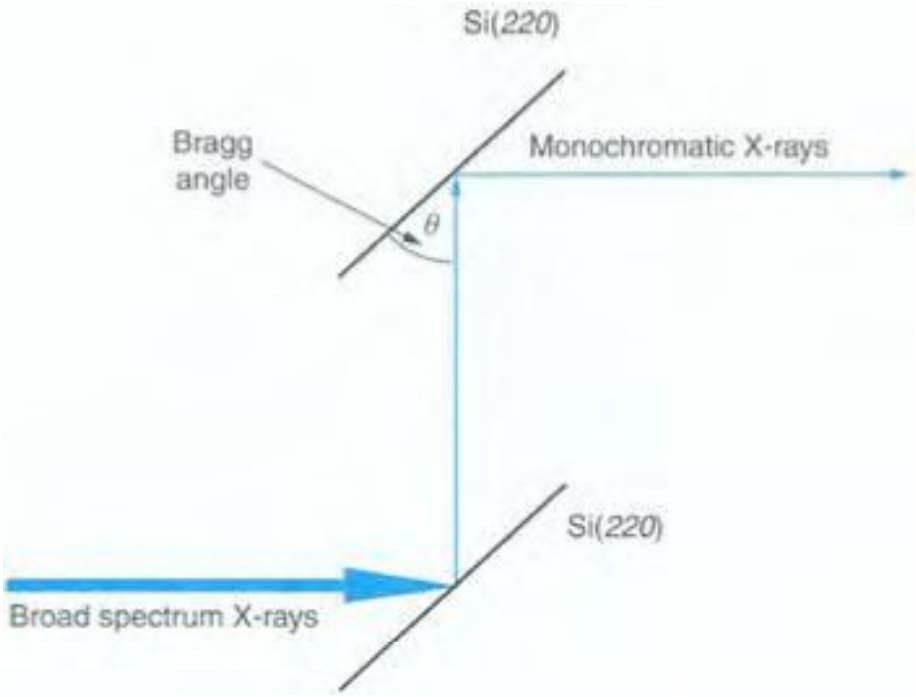

FIGURE 2.22 Bragg reflections from a double-crystal monochromator. From the Bragg equation, $n\lambda = 2d\sin\theta$, d for the planes of the crystal stays constant, so changing the angle changes the wavelength of the X-rays reflected.

Two crystals are used to make the exit beam parallel to the entrance beam. Curved crystals focus the X-rays.

The waves of the ejected photoelectron from the **K** shell can be thought of as a spherical wave emanating from the nucleus of the absorbing atom; this encounters neighbouring atoms and is partially scattered by them producing a phase shift (Figure 2.23). Depending on the phase shift experienced by the electron, the reflected waves can then interfere constructively or destructively with the outgoing wave, producing a net interference pattern at the nucleus of the original atom. Absorption by the original atom is now modified, and the effect is seen as sinusoidal oscillations or **fine structure** superimposed on the absorption edge (Figure 2.21) extending out to several hundred eV after the edge. The extent to which the outgoing wave is reflected by a neighbouring atom, and so the intensity of the reflected wave, is partly dependent

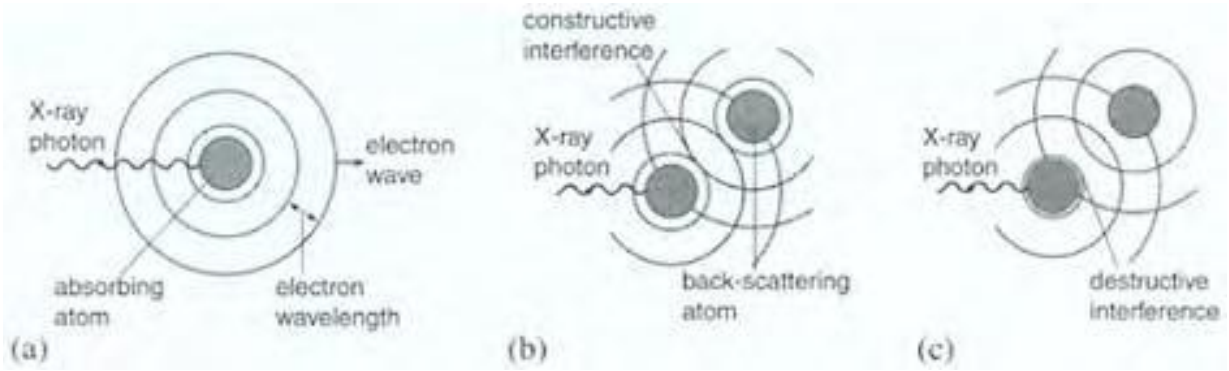

FIGURE 2.23 The EXAFS process: (a) the photoelectron is ejected by X-ray absorption, (b) the outgoing photoelectron wave (solid line) is backscattered constructively by the surrounding atoms (dashed line), and (c) destructive interference between the outgoing and the backscattered wave.

on the scattering factor of that atom. The interference pattern making up the EXAFS thus depends on the *number,* and the *type* of neighbouring atoms, and their *distance* from the absorbing atom.

The EXAFS function is obtained from the X-ray absorption spectrum by subtracting the absorption due to the free atom. A Fourier transform of the EXAFS data gives a **radial distribution function** which shows the distribution of the neighbouring atoms as a function of internuclear distance from the absorbing atom. Shells of neighbours, known as **coordination shells,** surround the absorbing atom. Finally, the radial distribution function is fitted to a series of trial structural models until a structure which best fits the

data is obtained, and the data is refined as a series of coordination shells surrounding the absorbing atom. The final structure will refine the number and types of atoms, and their distance from the absorbing atom. It is difficult to differentiate atoms of similar atomic number, and important to note that EXAFS only gives data on distance—no angular information is available. Depending on the quality of the data obtained, distances can be refined to about 1 pm, and in favourable cases several coordination shells out to about 600 pm can be refined.

In the example in Figure 2.24, a clay (a layered double hydroxide [LDH]) was intercalated with a transition metal complex $(NH_4)_2MnBr_4$. The EXAFS data in Figure 2.24(a) shows the Mn K-edge EXAFS of the pure complex, and we see one coordination sphere of four Br atoms at a distance of 2.49 Å, corresponding well to the tetrahedral coordination found in the X-ray crystal structure. However, after intercalation, the complex reacts with the layers in the clay, and the coordination changes to distorted octahedral where Mn is now surrounded by four O atoms at a distance of 1.92 Å and two Br atoms at a distance of 2.25 Å.

We saw earlier (Figure 2.9) that powder X-ray diffraction can be used to follow phase changes over time with heating; Figure 2.25 presents the corresponding iron K-edge EXAFS analysis for the same ferrosilicon sample. As the alpha ferrosilicon changes into the beta phase, a shell of eight silicon atoms at about 2.34 Å is found to surround Fe in both forms, but the beta form is found to have only two Fe atoms coordinated to Fe (2.97 Å), compared with 3.4 Fe atoms at 2.68 Å in the alpha phase.

X-rays are very penetrating, so EXAFS, like X-ray crystallography, examines the structure of the bulk of a solid. It has the disadvantage that it only provides information on interatomic distances, but has the considerable advantage that it is not confined to crystalline samples, and can be used on amorphous solids, glasses, and liquids. Not only that, but by using different absorption edges, it can investigate the coordination around more than one type of atom in the sample.

2.7.2 X-RAY ABSORPTION NEAR-EDGE STRUCTURE (XANES)

The precise position of the absorption edge varies with the chemical state of the absorbing atom, and this together with structure in the pre-edge region (Figure 2.21) can give information on the oxidation state of the atom and on its chemical environment. The example in Figure 2.26 depicts XANES spectra for manganese in different oxidation states.

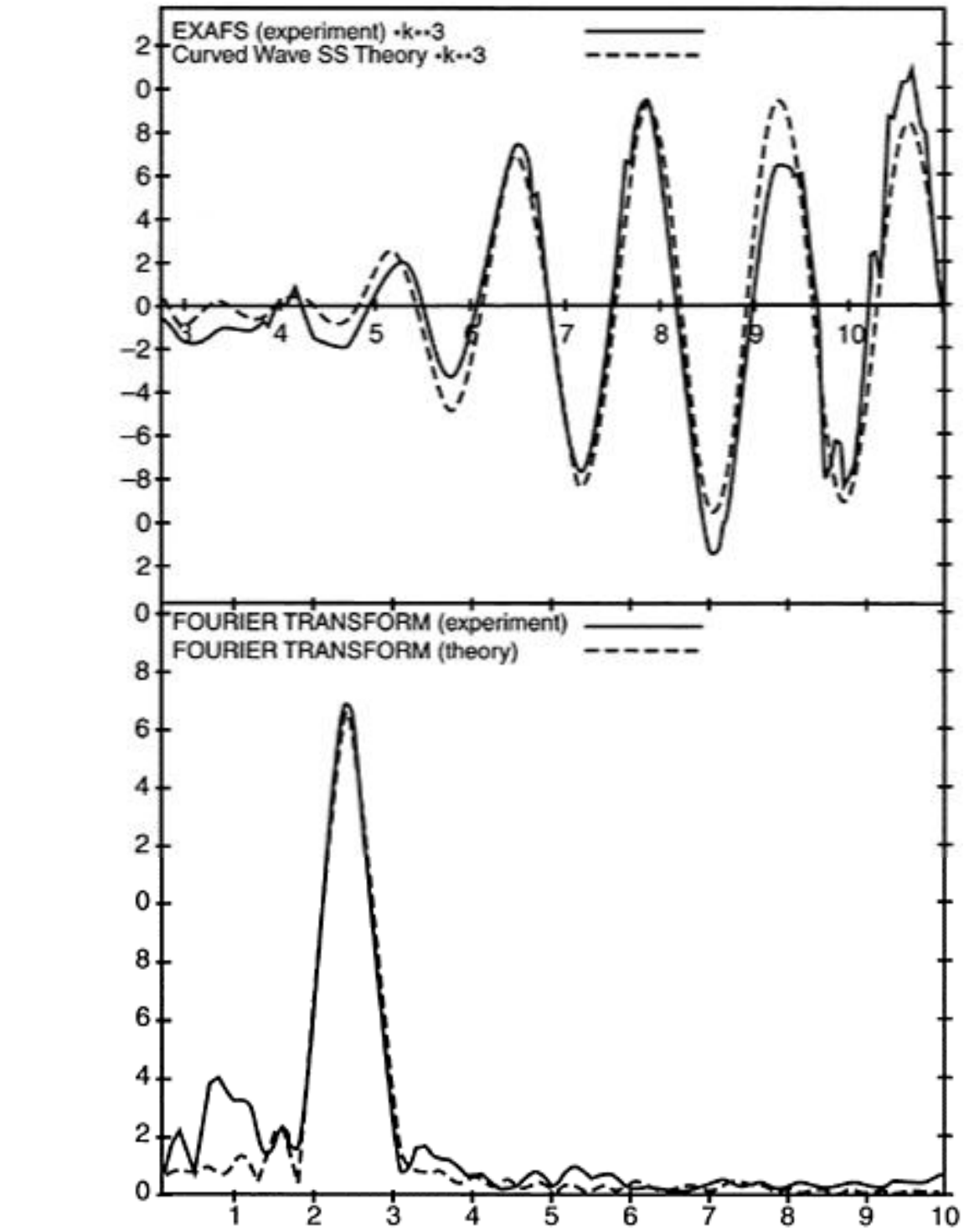

(a)

FIGURE 2.24 EXAFS data for (a) $(NH_4^+)_2MnBr_4^{2-}$: (upper) extracted EXAFS data; (lower) the radial distribution function, solid line experimental, dotted line calculated.

2.8 SOLID STATE NUCLEAR MAGNETIC RESONANCE SPECTROSCOPY (MAS NMR)

In solution NMR spectroscopy, dipolar interactions and anisotropic effects are averaged out by the molecular motion, but this is not so in the solid state, and the NMR spectra of solids tend to be broadened by three main effects:

1. **Magnetic dipolar interactions** can be removed by the application of a high power decoupling field at the resonance frequency.

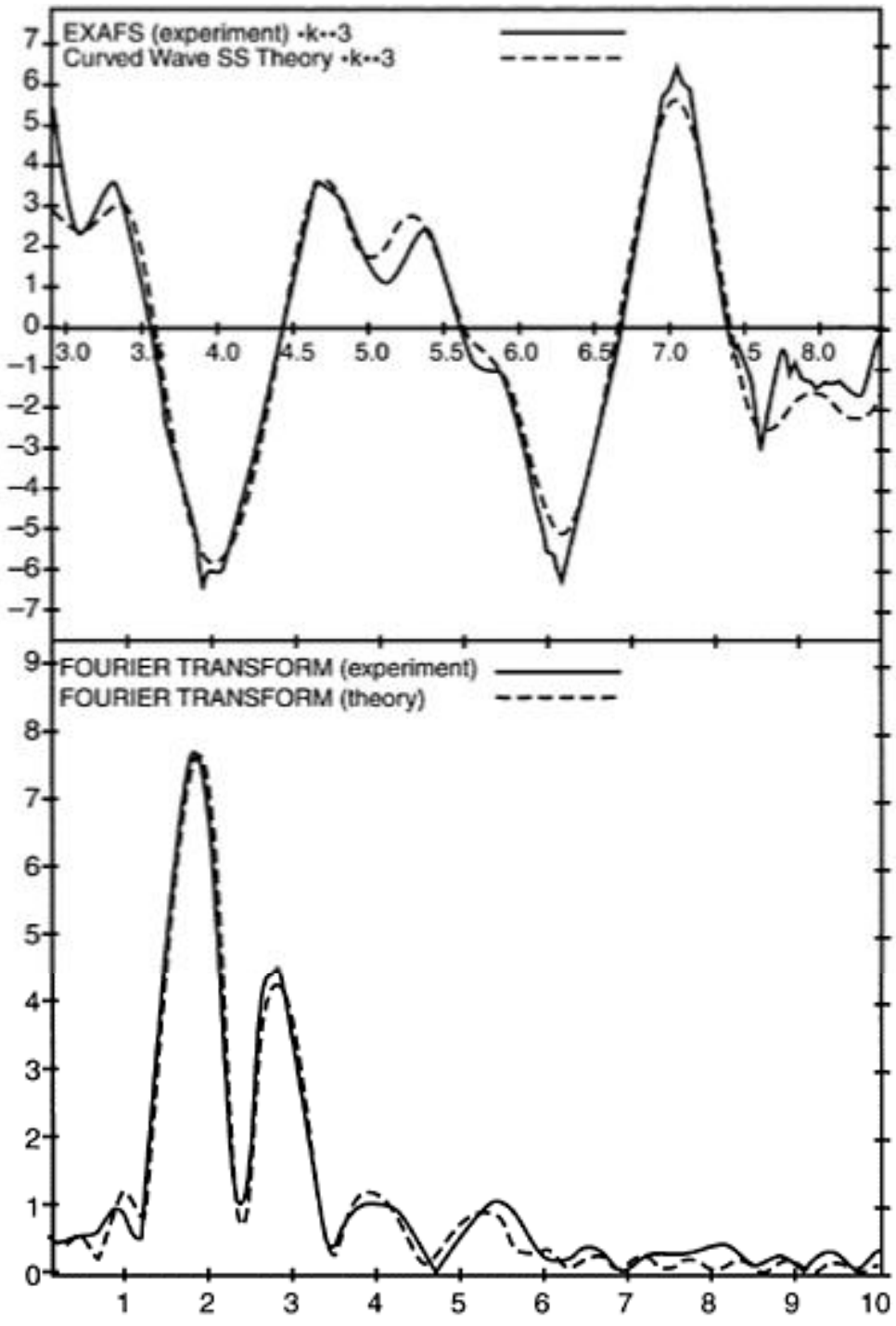

(b)

EXAFS data for (b) the intercalation of $MnBr_4^{2-}$ in a layered double hydroxide clay: (upper) extracted EXAFS data; (lower) the radial distribution function, solid line experimental, dotted line calculated.

2. Isotopes in low abundance have long spin-lattice relaxation times which give rise to poor signal-to-noise ratios. Sensitivity can be improved by using a technique known as **cross polarization** where a complex pulse sequence transfers polarization from an abundant nucleus to the dilute spin thereby enhancing the intensity of its signal.
3. The chemical shift of a particular atom varies with the orientation of the molecule to the field. In a solid this gives a range of values, an effect known as the **chemical shielding anisotropy**, which broadens the band.

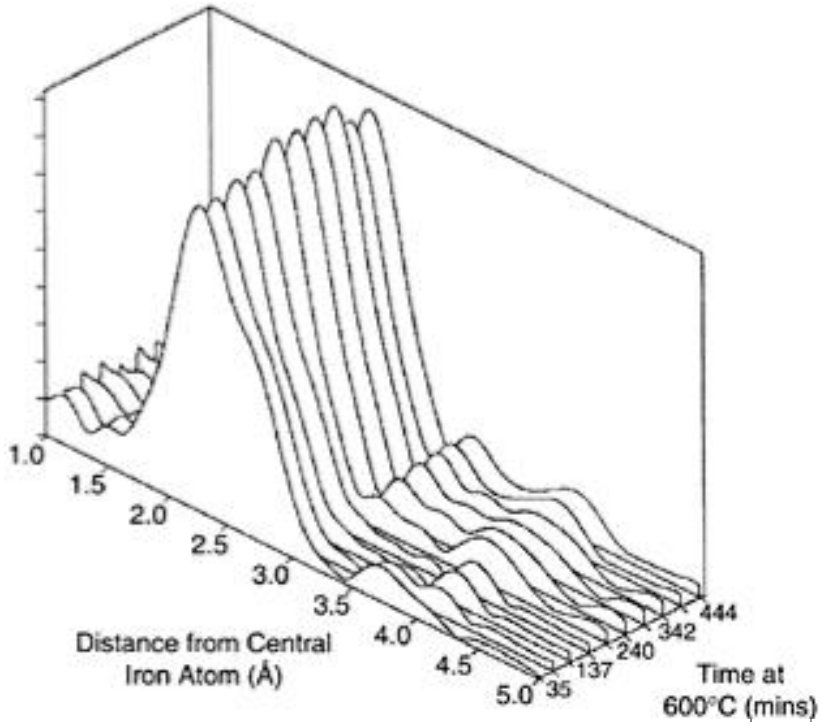

FIGURE 2.25 EXAFS patterns as a function of time illustrating the phase evolution of beta ferrosilicon from the alpha form when heated at 600°C. (Courtesy of Professor F.J.Berry, Open University.)

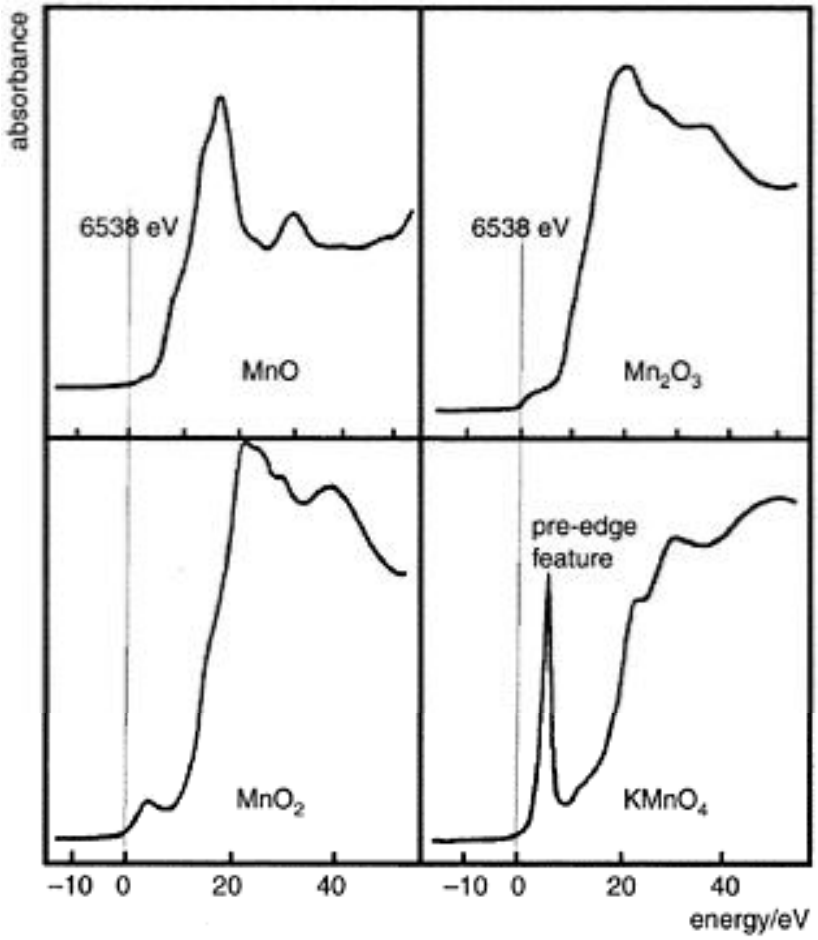

FIGURE 2.26 Mn K-edge XANES data for various manganese oxides. The vertical dashed line is the position of the metal edge. The position of the edge changes, and the pre-edge feature increases, with oxidation state. (Courtesy of Dr. Neville Greaves, University of Aberystwyth.)

The line broadening is due to anisotropic interactions, all of which contain a $(3\cos^2\theta-1)$ term. This term becomes zero when $3\cos^2\theta=1$, or $\cos\theta=(1/3)^{1/2}$, (i.e., $\theta=54°\ 44'$). **Magic angle spinning spectroscopy (MAS NMR)** spins the sample about an axis inclined at this so-called **magic angle** to the direction of the magnetic field and eliminates these sources of broadening, improving the resolution in chemical shift of the spectra. The spinning speed has to be greater than the frequency spread of the signal, if it is less, as may be the case for very broad bands, then a set of so-called "spinning side-bands" are observed, and care is needed in assigning the central resonance.

MAS NMR is often used nowadays as an umbrella term to imply the application of any or all of these techniques in obtaining a solid state NMR spectrum. High resolution

spectra can be measured for most spin I=½ isotopes. MAS NMR has proved very successful in elucidating zeolite structures. Zeolites are three-dimensional framework silicate structures where many of the silicon sites are occupied by aluminium. Because Al and Si are next to each other in the Periodic Table they have similar X-ray atomic scattering factors, and consequently are virtually indistinguishable based on X-ray crystallographic data. It is possible to build up a picture of the overall shape of the framework with accurate atomic positions but not to decide which atom is Si and which is Al.

^{29}Si has a nuclear spin I=½ and so gives sharp spectral lines with no quadrupole broadening or asymmetry; the sensitivity is quite high and ^{29}Si has a natural abundance of 4.7%. Pioneering work using MAS NMR on zeolites was carried by E. Lippmaa and G.Engelhardt in the late 1970s. They demonstrated that up to five peaks could be observed for the ^{29}Si spectra of various zeolites and that these corresponded to the five different Si environments that can exist. Each Si is coordinated by four oxygen atoms, but each oxygen can then be attached either to a Si or to an Al atom giving the five possibilities: $Si(OAl)_4$, $Si(OAl)_3(OSi)$, $Si(OAl)_2(OSi)_2$, $Si(OAl)(OSi)_3$, and $Si(OSi)_4$. Most importantly, they also demonstrated that characteristic ranges of these shifts could be assigned to each coordination type. These ranges could then be used in further structural investigations of other zeolites (Figure 2.27). A MAS NMR spectrum of the zeolite known as analcite is depicted in Figure 2.28. Analcite has all five possible environments. Even with this information, it is still an extremely complicated procedure to decide where each linkage occurs in the structure.

^{27}Al has a 100% natural abundance and a nuclear spin $I = \frac{5}{2}$, resulting in a strong resonance which is broadened and rendered asymmetric by second-order quadrupolar effects. However, determining the ^{27}Al MAS NMR spectrum of a zeolite can still have great diagnostic value because it distinguishes different types of aluminium coordination: octahedrally coordinated $[Al(H_2O)_6]^{3+}$ is frequently trapped as a cation in the pores of zeolites and gives a peak at about 0 ppm ($[Al(H_2O)_6]^{3+}$(aq) is used as the reference); tetrahedral $Al(OSi)_4$ gives rise to a single resonance with characteristic Al chemical shift values for individual zeolites in the range of 50 to 65 ppm; and $AlCl_4^-$, which may be present as a residue from the preparative process, has a resonance at about 100 ppm.

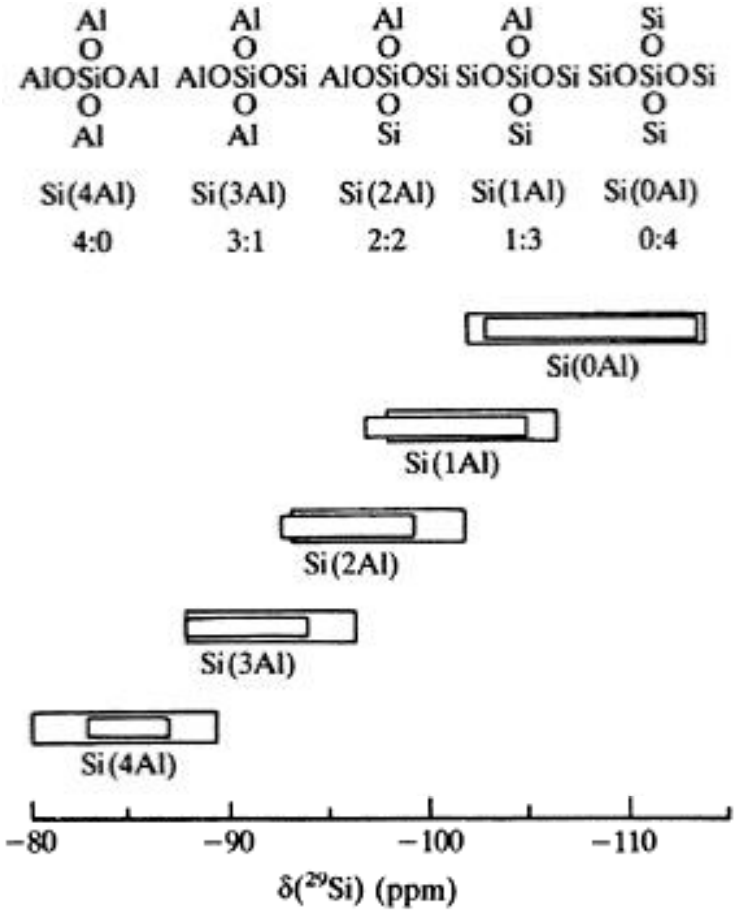

FIGURE 2.27 The five possible local environments of a silicon atom together with their characteristic chemical shift ranges. The inner boxes represent the ^{29}Si shift ranges suggested in the earlier literature. The outer boxes represent the extended ^{29}Si shift ranges which are more unusual.

2.9 THERMAL ANALYSIS

Thermal analysis methods investigate the properties of solids as a function of a change in temperature. They are useful for investigating phase changes, decomposition, loss of water or oxygen, and for constructing phase diagrams.

2.9.1 DIFFERENTIAL THERMAL ANALYSIS (DTA)

A phase change produces either an absorption or an evolution of heat. The sample is placed in one chamber, and a solid that will not change phase over the temperature range of the experiment in the other. Both chambers are heated at a controlled uniform rate in a

furnace, and the difference in temperature between the two is monitored and recorded against time. Any reaction in the sample will be represented as a peak in the plot of differential temperature; exothermic reactions give an increase in temperature, and endothermic a decrease, so the peaks appear in opposite directions. Figure 2.29 depicts three exotherms in the DTA of KNO_3, due to (i) a phase change from tetragonal to trigonal at 129°C, (ii) melting at 334°C, and (iii) decomposition above 550°C.

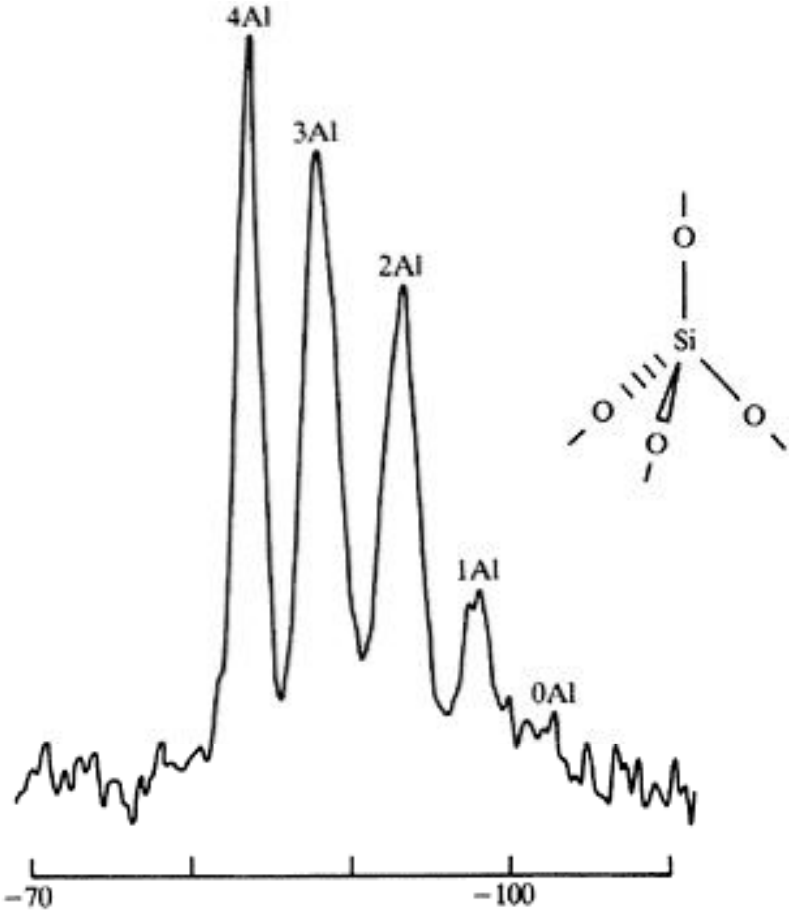

FIGURE 2.28 ^{29}Si MAS NMR spectrum at 79.6 MHz of analcite, illustrating five absorptions characteristic of the five possible permutations of Si and Al atoms attached at the corners of

2.9.2 THERMOGRAVIMETRIC ANALYSIS (TGA)

In this experiment, the weight of a sample is monitored as a function of time as the temperature is increased at a controlled uniform rate. The loss of water of crystallization or volatiles such as oxygen shows up as a weight loss, as does decomposition. Oxidation or adsorption of gas shows up as a weight gain. The TGA plot for KNO_3 in Figure 2.29

depicts a small weight loss up to about 550°C, probably due to the loss of adsorbed water, followed by a dramatic weight loss when the sample decomposes.

2.9.3 DIFFERENTIAL SCANNING CALORIMETRY (DSC)

DSC measures the amount of heat released by a sample as the temperature is increased or decreased at a controlled uniform rate, and so can investigate chemical reactions and measure heats of reaction for phase changes (Figure 2.30).

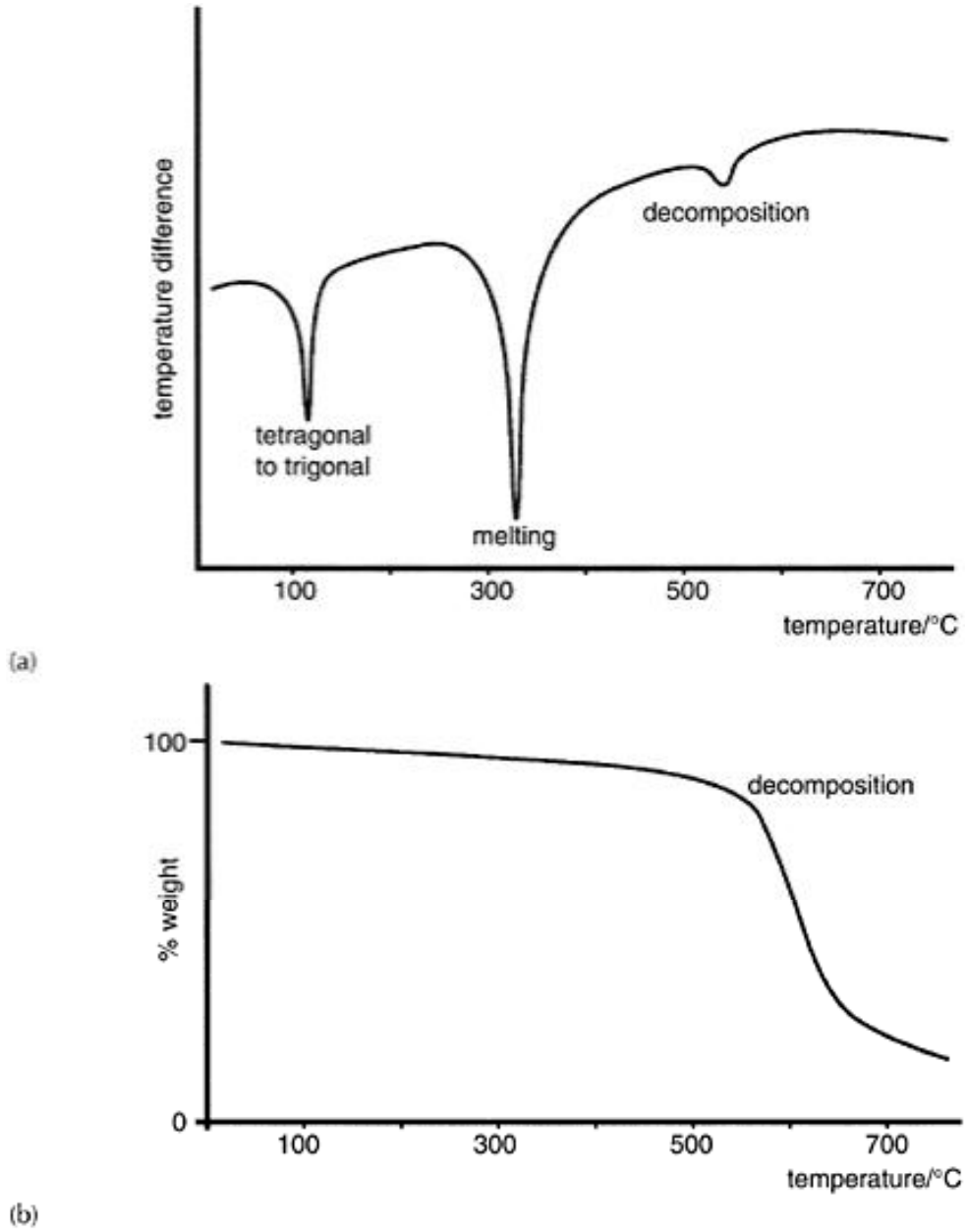

FIGURE 2.29 (a) The DTA trace for KNO_3; (b) the TGA trace for KNO_3.

2.10 SCANNING TUNNELLING MICROSCOPY (STM) AND ATOMIC FORCE MICROSCOPY (AFM)

In **scanning tunnelling microscopy (STM),** a sharp metal tip is brought sufficiently close to the surface of the solid sample (0.5–1 nm) that their electron-wave functions can overlap and electrons tunnel between the two. When a potential is applied to the solid surface, the electrons flow between the tip and the solid to give a tunnelling current in the range of pico to nano amperes. The magnitude of the current is very sensitive to the size of the gap, changing by a factor of 10 when the distance changes by 100 pm. The metal tip is scanned backward and forward across the solid, and the steep variation of the tunnelling current with distance gives an image of the atoms on the surface. The image is usually formed by keeping a constant tunnelling current and measuring the distance, thus creating contours of constant density of states on the surface. By changing the sign of the potential, the tunnelling direction reverses, and thus STM can map either occupied or unoccupied density of states. The map thus illustrates features due to both the topography and to the electronic structure, and can illustrate the positions of individual atoms (Figure 2.31(a)).

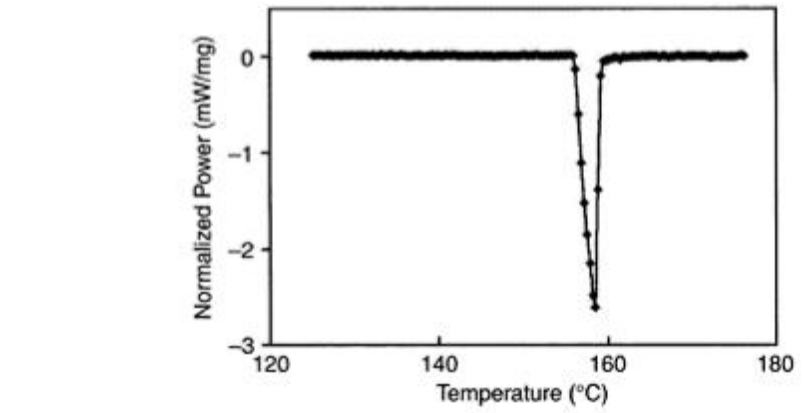

(a)

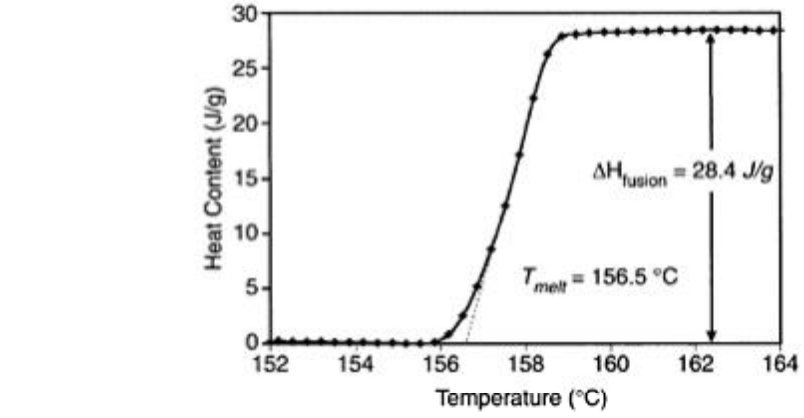

(b)

FIGURE 2.30 (a) DSC trace for the melting of indium metal; (b) integration of the power data to give

the heat of fusion for In. (Courtesy of Dr. Albert Sacco Jr., Northeastern University, Boston, Massachusetts.)

AFM is based on the detection of very small (of the order of nano newtons) forces between a sharp tip and atoms on a surface (Figure 2.31(b–d)). The tip is scanned across the surface at subnanometer distances, and the deflections due to attraction or repulsion by the underlying atoms detected. The technique produces atomic scale maps of the surface.

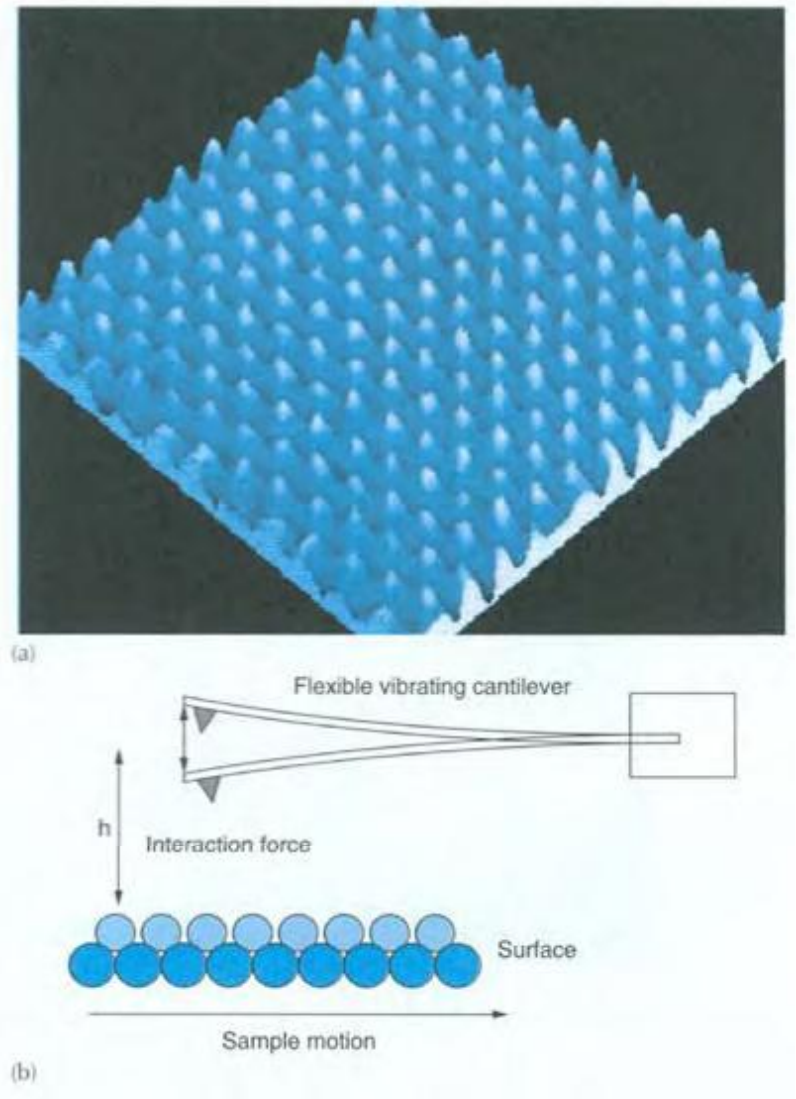

FIGURE 2.31 (a) STM image of a periodic array of C atoms on HOPG. (Courtesy of Prof. R.Reifenberger, Purdue University.) (b) Diagram of AFM.

2.11 TEMPERATURE PROGRAMMED REDUCTION (TPR)

Temperature programmed reduction measures the reaction of hydrogen with a sample at various temperatures. The results are interpreted in terms of the different species present in the sample and their amenability to reduction. Therefore, these results can give information on the presence of different oxidation states or the effect of a dopant in a lattice. It is useful for measuring the temperature necessary for the complete reduction of a catalyst and is commonly used to investigate the interaction of a metal catalyst with its support, or of the effect of a promoter on a metal catalyst.

The sample is heated over time in a furnace under a flowing gas mixture, typically 10% H_2 in N_2. Hydrogen has a high electrical conductivity, so a decrease in hydrogen concentration is marked by a decrease in conductivity of the gas mixture. This change is measured by a thermal conductivity cell (katharometer) and is recorded against either time or temperature.

The peaks in a TPR profile (Figure 2.32) measure the temperature at which various reduction steps take place. The amount of hydrogen used can be determined from the area under the peak. In the example, we see two peaks, indicating that the reduction of Fe_2O_3 takes place in two stages, first to Fe_3O_4 and then to metallic Fe.

Other temperature-programmed techniques include Temperature Programmed Oxidation and Sulfidation (TPO and TPS) for investigating oxidation and sulfidation behaviour, and Temperature Programmed Desorption (TPD) (also called Thermal Desorption Spectroscopy [TDS]), which analyses gases desorbed from the surface of a solid or a catalyst on heating.

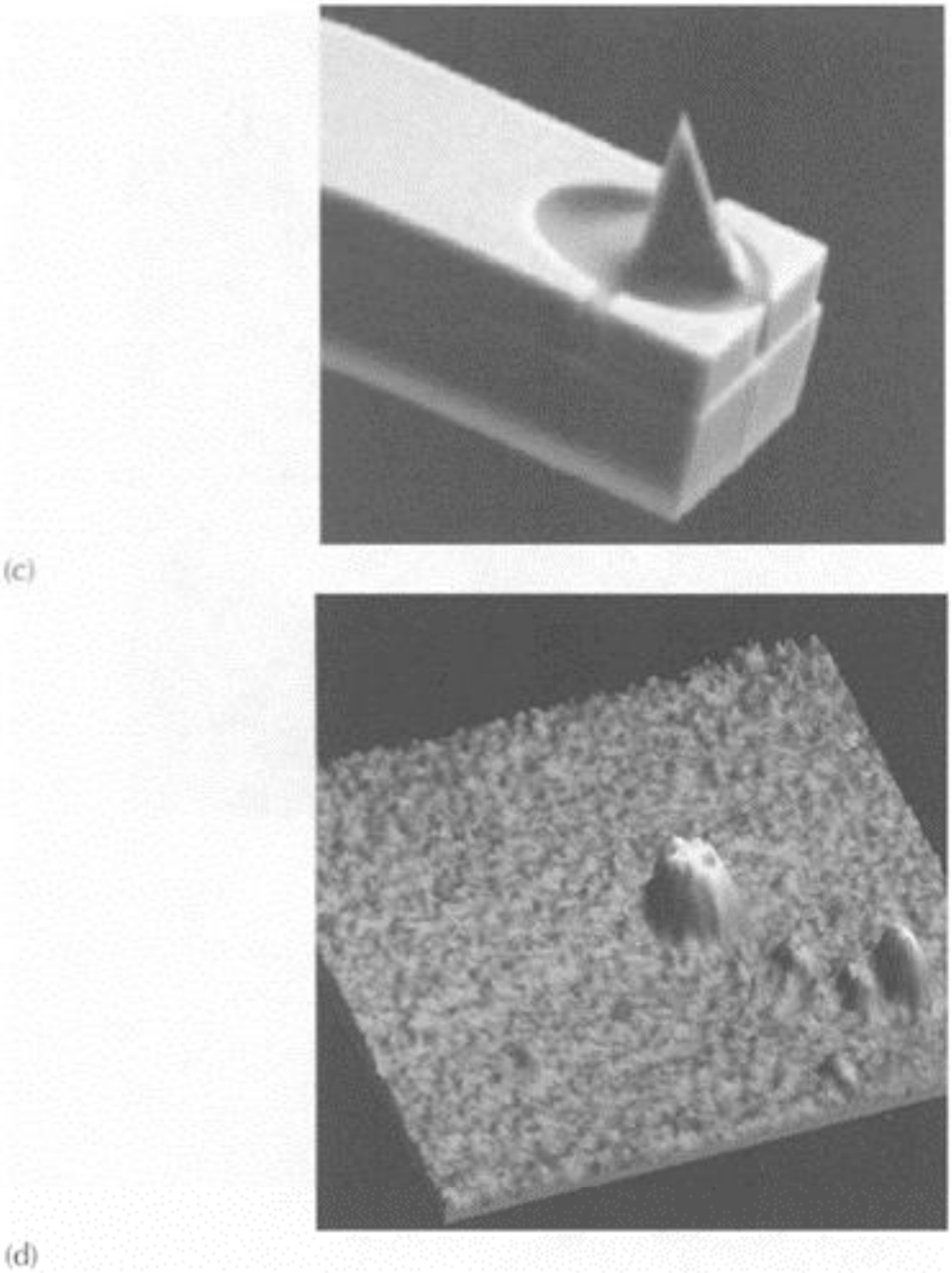

(c) AFM diamond tip on a silicon cantilever, and (d) AFM image of gold cluster on an oxidized surface. (Courtesy of Prof. R.Reifenberger, Purdue University.)

2.12 OTHER TECHNIQUES

In an introductory general text such as this, it is impossible to do justice to the plethora of physical techniques which are currently available to the solid state chemist. We have therefore concentrated on those which are most widely available, and on those which examine bulk material rather than surfaces. For these reasons, we have not covered Mössbauer spectroscopy, electron spectroscopies (XPS, UVPS, AES, and EELS) or low

energy electron diffraction (LEED); for these, you will need to refer to more specialized texts. We have also not covered vibrational spectroscopy (IR and

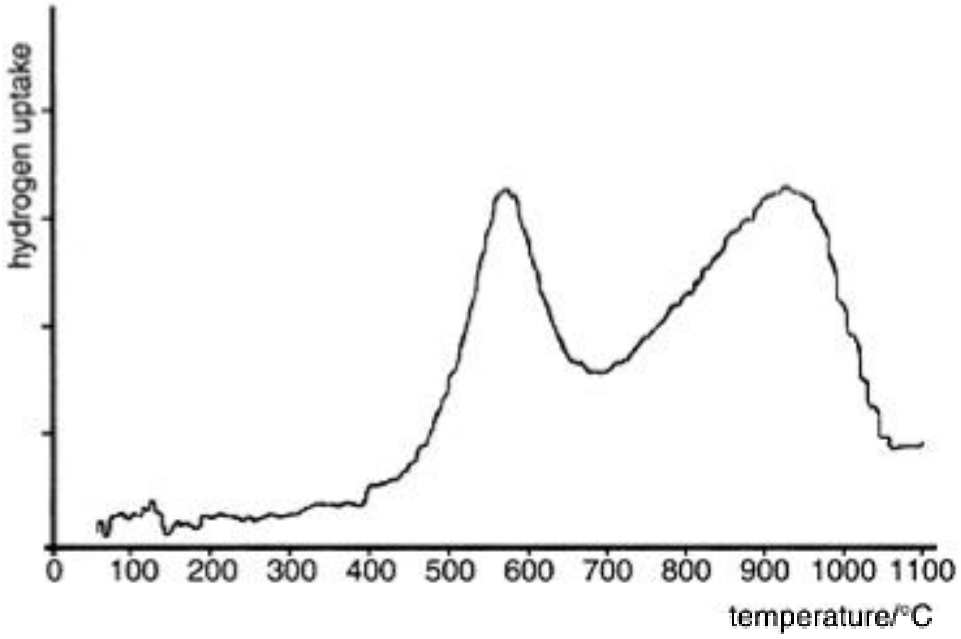

FIGURE 2.32 TPR trace for α-Fe_2O_3.

Raman) as good treatments of this subject are to be found in most undergraduate physical chemistry texts.

QUESTIONS

1. What are the spacings of the *100, 110,* and *111* planes in a cubic crystal system of unit cell dimension *a*? In what sequence would you expect to find these reflections in a powder diffraction photograph?

2. What is the sequence of the following reflections in a primitive cubic crystal: *220, 300,* and *211*?

3. Nickel crystallizes in a cubic crystal system. The first reflection in the powder pattern of nickel is the *111*. What is the Bravais lattice?

4. The $\sin^2\theta$ values for Cs_2TeBr_6 are listed in Table 2.4 for the observed reflections. To which cubic class does it belong? Calculate its unit-cell length assuming Cu-K_α radiation of wavelength 154.2 pm.

TABLE 2.4 $\sin^2\theta$ values for Cs_2TeBr_6

$\sin^2\theta$
.0149
.0199
.0399
.0547
.0597
.0799
.0947

TABLE 2.5 θ values for NaCl

θ_{hkl}
13°41′
15°51′
22°44′
26°56′
28° 14′
33°7′
36°32′
37°39′
42°0′
45°13′
50°36′
53°54′
55°2′
59°45′

5. X-ray powder data for NaCl is listed in Table 2.5. Determine the Bravais lattice, assuming that it is cubic.

6. Use the data given in Question 5 to calculate a unit-cell length for the NaCl unit cell.

7. If the unit cell length of NaCl is a=563.1 pm and the density of NaCl is measured to be 2.17×10^3 kg m^{-3}; calculate Z, the number of formula units in the unit cell. (The atomic masses of sodium and chlorine are 22.99 and 35.45, respectively.)

8. A powder diffraction pattern establishes that silver crystallizes in a face-centred cubic unit cell. The *111* reflection is observed at θ=19.1°, using Cu-K_α radiation. Determine the unit cell length, a. If the density of silver is 10.5×10^3 kg m^{-3} and Z=4, calculate the value of the Avogadro constant. (The atomic mass of silver is 107.9.)

9. Calcium oxide crystallizes with a face-centred cubic lattice, a=481 pm and a density $\rho=3.35\times10^3$ kg m^{-3}: calculate a value for Z. (Atomic masses of Ca and O are 40.08 and 15.999, respectively.)

10. Thorium diselenide, $ThSe_2$, crystallizes in the orthorhombic system with a= 442.0 pm, b=761.0 pm, c=906.4 pm and a density $\rho=8.5\times10^3$ kg m^{-3}: calculate Z. (Atomic masses of Th and Se are 232.03 and 78.96, respectively.)

11. Cu crystallizes with a cubic close-packed structure. The Bragg angles of the first two reflections in the powder pattern collected using Cu-K_α radiation are 21.6° and 25.15°. Calculate the unit cell length a, and estimate a radius for the Cu atom.

12. Arrange the following atoms in order of their ability to scatter X-rays: Na, Co, Cd, H, T1, Pt, Cl, F, O.

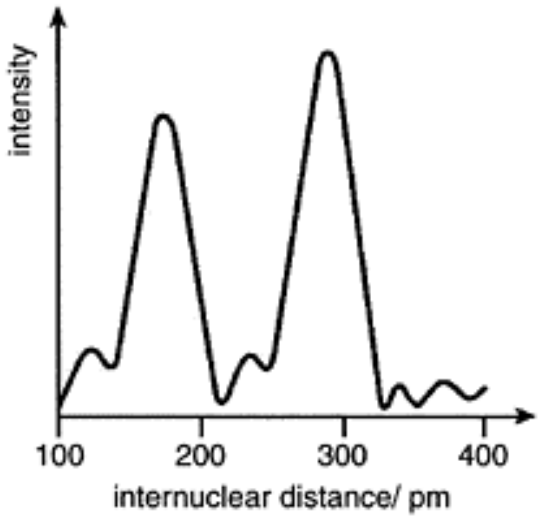

FIGURE 2.33 Co edge EXAFS radial distribution function for $Co(CO)_4$.

13. In a cubic crystal we observe the *111* and *222* reflections, but not *001*. What is the Bravais lattice?

14. Interpret the EXAFS radial distribution function for $Co(CO)_4$ shown in Figure 2.33.

15. Figure 2.34 illustrates the ^{79}Si MAS NMR spectrum of the zeolite faujasite. Use this figure to determine which Si environments are most likely to be present.

16. Figure 2.35 illustrates the ^{29}Si spectrum of the same sample of faujasite as Figure 2.34, but after treatment with $SiCl_4$ and washing with water. What has happened to it?

17. A sample of faujasite was treated with $SiCl_4$ and four $^{27}A1$ MAS NMR spectra were taken at various stages afterwards (Figure 2.36). Describe carefully what has happened during the process.

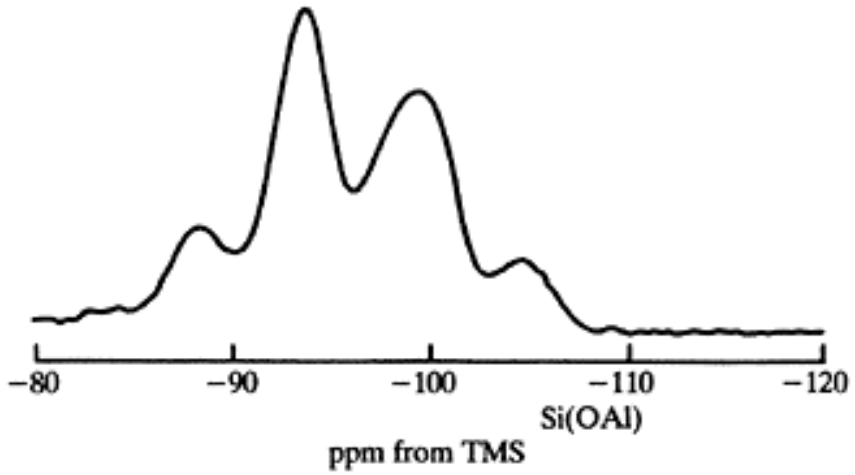

FIGURE 2.34 ^{29}Si MAS NMR spectrum at 79.6 MHz of faujasite of Si/Al=2.61 (zeolite-Y).

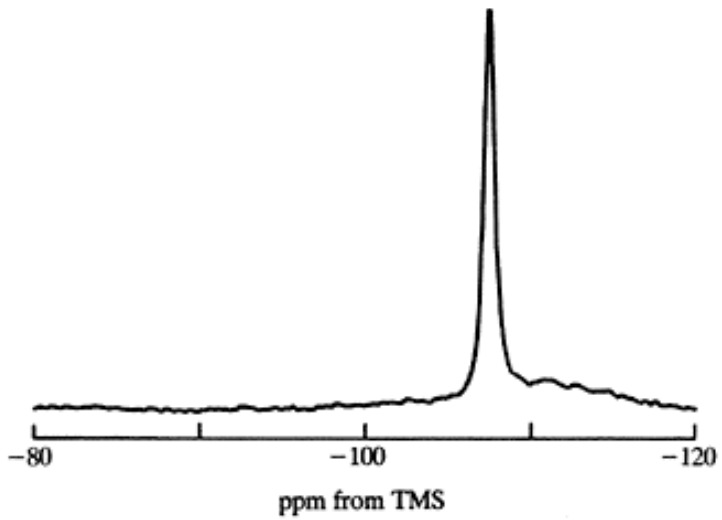

FIGURE 2.35 ^{29}Si MAS NMR spectrum at 79.6 MHz of faujasite of Si/Al=2.61 after successive

dealumination with $SiCl_4$ and washings.

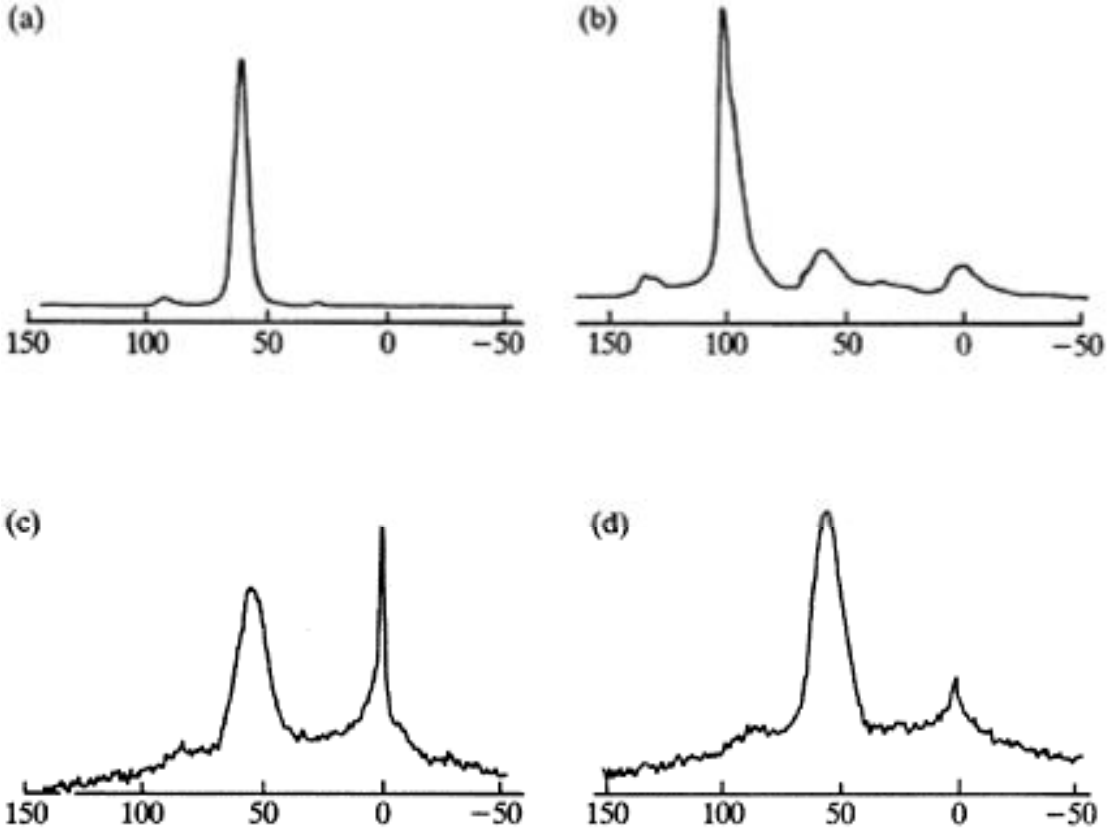

FIGURE 2.36 ^{27}Al MAS NMR spectra at 104.2 MHz obtained on faujasite samples at various stages of the $SiCl_4$ dealumination procedure: (a) starting faujasite sample, (b) intact sample after reaction with $SiCl_4$ before washing, (c) sample (b) after washing with distilled water, and (d) after several washings.

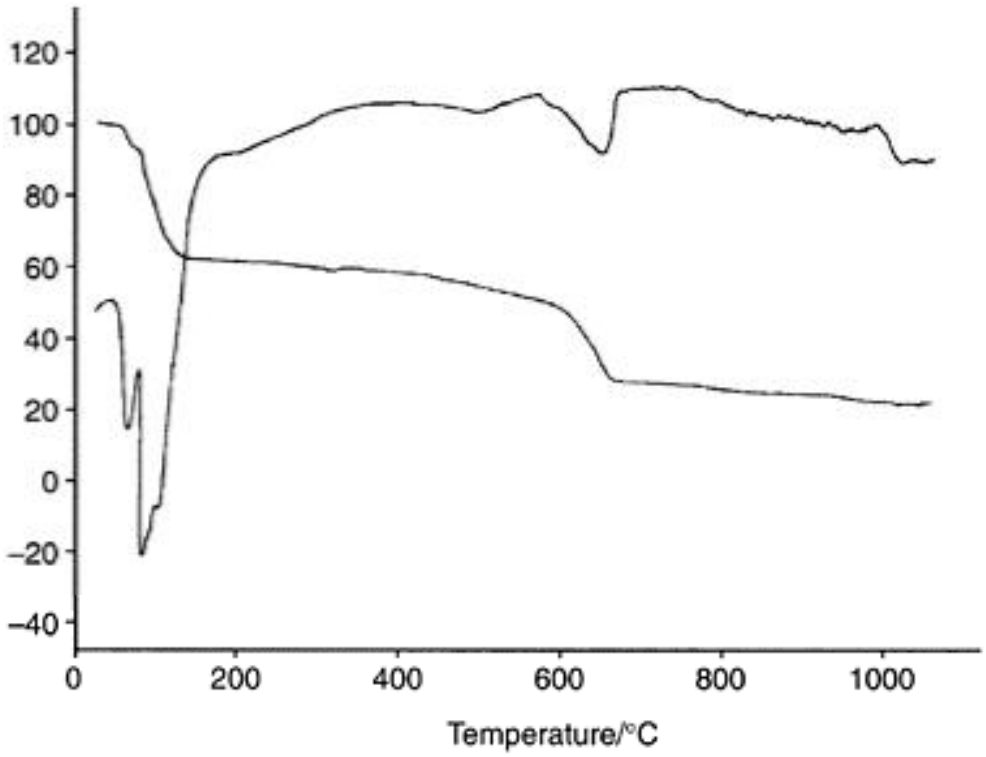

FIGURE 2.37 DTA and TGA traces for ferrous sulfate heptahydrate.

18. A TGA trace for 25 mg of a hydrate of manganese oxalate, $MnC_2O_4.xH_2O$, revealed a weight loss of 20 mg at 100°C. What was the composition of the hydrate? A further weight loss occurs at 250°C, but then a weight *gain* at 900°C. What processes might be taking place?

19. Figure 2.37 illustrates the DTA and TGA traces for ferrous sulfate heptahydrate. Describe what processes are taking place.